HHS Public Access

Author manuscript

Acta Biomater. Author manuscript; available in PMC 2022 February 01.

Published in final edited form as:

Acta Biomater. 2021 February ; 121: 431–443. doi:10.1016/j.actbio.2020.11.025.

COMPARISON OF MORPHOMETRIC, STRUCTURAL, MECHANICAL, AND PHYSIOLOGIC CHARACTERISTICS OF HUMAN SUPERFICIAL FEMORAL AND POPLITEAL ARTERIES

Majid Jadidi[a], **Sayed Ahmadreza Razian**[b], **Eric Anttila**[a], **Tyler Doan**[b], **Josiah Adamson**[b], **Margarita Pipinos**[b], **Alexey Kamenskiy**[b,*]

[a]Department of Mechanical and Materials Engineering, University of Nebraska-Lincoln, Lincoln, NE

[b]Department of Biomechanics, University of Nebraska Omaha, Omaha, NE

Abstract

Peripheral arterial disease differentially affects the superficial femoral (SFA) and the popliteal (PA) arteries, but their morphometric, structural, mechanical, and physiologic differences are poorly understood. SFAs and PAs from 125 human subjects (age 13–92, average 52±17 years) were compared in terms of radii, wall thickness, and opening angles. Structure and vascular disease were quantified using histology, mechanical properties were determined with planar biaxial extension, and constitutive modeling was used to calculate the physiologic stress-stretch state, elastic energy, and the circumferential physiologic stiffness. SFAs had larger radii than PAs, and both segments widened with age. Young SFAs were 5% thicker, but in old subjects the PAs were thicker. Circumferential (SFA: 96→193°, PA: 105→139°) and longitudinal (SFA: 139→306°, PA: 133→320°) opening angles increased with age in both segments. PAs were more diseased than SFAs and had 11% thicker intima. With age, intimal thickness increased 8.5-fold, but medial thickness remained unchanged (620μm) in both arteries. SFAs had 30% more elastin than the PAs, and their density decreased ~50% with age. SFAs were more compliant than PAs circumferentially, but there was no difference longitudinally. Physiologic circumferential stress and stiffness were 21% and 11% higher in the SFA than in the PA across all ages. The stored elastic energy decreased with age (SFA: 1.4→0.4kPa, PA: 2.5→0.3kPa). While the SFA and PA demonstrate appreciable differences, most of them are due to vascular disease. When pathology is the same, so are the mechanical properties, but not the physiologic characteristics that remain distinct due to geometrical differences.

Graphical Abstract

[*]Correspondence and Reprints requests to: Department of Biomechanics, Biomechanics Research Building, University of Nebraska at Omaha. akamenskiy@unomaha.edu.

Declaration of competing interests

None

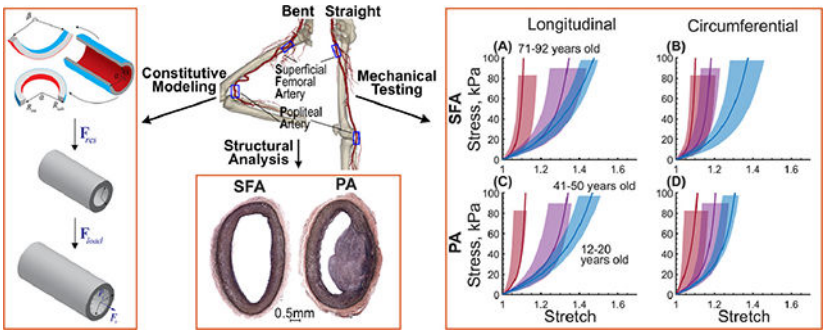

Keywords

superficial femoral artery; popliteal artery; mechanical properties; constitutive modeling; aging; regional differences

1 INTRODUCTION

Peripheral arterial disease (PAD) is often caused by an atherosclerotic obstruction of the femoropopliteal artery (FPA) in the lower limb[1]. It is a major public health burden and is associated with high morbidity, mortality, and impairment in life quality[2–5]. Surgical and interventional therapies for PAD are notorious for high failure rates[6–21], and lower blood flow[22–27] and the large deformations experienced during flexion of the limbs[26–37] are likely involved. Significant efforts are focused on the development of better materials and devices to improve clinical outcomes of PAD repair[11,35,38–40], and detailed information on the morphometric, structural, mechanical, and physiologic FPA characteristics can guide these developments.

The FPA begins as the common femoral artery (Figure 1) and continues as the superficial femoral artery (SFA) into the upper thigh. It becomes the popliteal artery (PA) as it traverses the adductor hiatus (AH), a gap between the adductor magnus muscle and the femur, passing from the anterior thigh posteriorly into the popliteal fossa behind the knee. Clinically, the two principal sites of FPA occlusions are the artery at the AH and the PA behind the knee[41] (Figure 1).

We have recently reported the mechanical and structural characteristics of human FPAs in a wide range of ages[26,42–46], but studies of how these characteristics change along the length of the artery were limited to small sample sizes[47,48], were not done using arteries from the same subjects, and, most importantly, have not considered the effects of vascular disease. The goal of the current work was to evaluate SFAs and PAs obtained from the same human subjects in a wide range of ages, and compare them in terms of morphometric, structural, mechanical, and physiologic characteristics while controlling for the degree of vascular disease. This was achieved by using imaging and bidirectional histology, planar biaxial mechanical testing, and constitutive modeling. Data informing the regional differences between the two FPA segments that typically experience different flow and mechanical deformations during limb flexion (Figure 1A) and are differentially affected by vascular disease (Figure 1B), may help better understand the mechanophysiology of the

lower extremity vasculature, guide the development and refinement of computational models that evaluate arterial mechanics, hemodynamics, and device-artery interactions[26,27,34,35,49–51], and help develop new materials and devices for PAD repair.

2 METHODS

2.1 Arterial specimens

The FPAs from the profunda femoris artery to the tibioperoneal trunk (Figure 1) were obtained from 125 tissue donors 13–92 years old (average age 52±17 years, 71% male) by an organ procurement organization Live On Nebraska after obtaining consent from next of kin, and were tested within 4 hours of procurement to preserve freshness. Demographics and risk factors of the subjects are summarized in Table 1. Prior to excision, the *in situ* longitudinal pre-stretch of the entire FPA was measured using an umbilical tape[43]. Proximal SFA 1 cm distal to the profunda femoris artery, and distal PA 1 cm proximal to the tibioperoneal trunk (Figure 1), were obtained from the FPA and kept in 0.9% phosphate-buffered saline during all experiments. Morphometric measurements were obtained optically while the specimens freely floated in saline. They included the outer radius of the *load-free* arterial ring ρ_{adv}, the inner and outer radii (R_{int}, R_{adv}) and thickness of the *stress-free* radially-cut arterial ring, and the circumferential (α) and longitudinal (β) opening angles in the *stress-free* configuration (Figure 2)[42,47]. Opening angles were measured by selecting three points on the stress-free section (one in the middle and two close to the ends), and then fitting a circle through these points (Figure 2, green lines). Since the diseased specimens often had nonuniform thickness, the thickness was assessed in at least 10 different locations across the circumference before reporting the average value.

2.2 Histological Analysis

The intramural structure of the SFA and PA specimens was evaluated using bidirectional histology and arterial sections immediately adjacent to the morphometrically-measured and mechanically-tested specimens. Arterial cross-sections and ~1cm longitudinal strips were fixed in methacarn, dehydrated in 70% ethanol, embedded in paraffin, sectioned using a microtome, and stained with Verhoeff-Van Gieson (VVG) stain. Intimal and medial layer thicknesses and the density of elastin were measured on both transverse and longitudinal sections using a semi-automated custom-made software written in Visual Studio C# with .Net 4.6.2 framework and OpenCV libraries. This software allowed the selection of the layer boundaries in the entire histological slide, so the thickness and density measures represented the entire arterial section as opposed to a few discrete measurements.

The degree of vascular disease in each specimen was quantified using a six-stage scale[43,44] (Figure 3), and all grading was done by a single operator to reduce variability. Stage I represented healthy arteries with no intimal thickening, no lipid pools, and no calcification; stage II included arteries with minor intimal thickening and some smooth muscle cell (SMC) proliferation, but no protruding plaques; stage III arteries had plaques with minor protrusion into the lumen, and possibly small pools of extracellular lipid, but no calcium; stage IV represented samples with minor calcification, a protruding plaque with <30% stenosis, and moderate pools of extracellular lipid; stage V included arteries with

severe medial calcification, stenosis >75%, or aneurysmal dilation, and possibly large pools of extracellular lipid; lastly, stage VI represented the most severely diseased arteries with extremely calcified arterial medial layer, total vessel occlusions, or fully-developed aneurysms.

In addition to the degree of vascular disease, we have also quantified the discontinuity of elastic fibers in the external elastic lamina (EEL) using a previously reported five-stage scale[44] (Figure 4), and have counted the number of major breaks in the EEL according to Figure 5. The elastic fiber discontinuity scale ranged from 1 (fully continuous fibers) to 5 (completely discontinuous fibers), and the number of major breaks ranged from none to ≥4.

2.3 Planar Biaxial Testing

Planar biaxial tests were performed on fresh SFA and PA specimens sprinkled with graphite markers to allow measurements of the deformation gradient. Test axes were aligned with the longitudinal and circumferential directions of the artery, and the specimens were attached using rakes as previous studies demonstrated negligible shear[47,48]. All arteries were preloaded with 0.02–0.1N force, subjected to 20 equibiaxial cycles of preconditioning, and when the curves became repeatable, a total of 21 stretch-controlled multi ratio protocols ranging from 1:0.1 to 1:0.9 and from 0.9:1 to 0.1:1 with 0.1 step and three equibiaxial 1:1 stability checks at 0.01 s^{-1} strain rate were applied to obtain sufficient data density for constitutive modeling. Biaxial forces and stretches were recorded, and used to calculate the experimental Cauchy stresses[52]. More details of these tests can be found in our previous works[47,48,52].

2.4 Constitutive Modeling

Experimental data were used to determine the constitutive parameters for the four-fiber family invariant-based model previously shown to accurately portray the behavior of human FPAs of different ages[42,47,48,52]. For this model, the strain energy function W is given by:

$$W = \frac{c_{gr}}{2}(I_{\boldsymbol{C}} - 3) + \sum_{i=1}^{4} \frac{c_1^i}{4c_2^i}\left(e^{c_2^i\left\langle IV_{\boldsymbol{C}}^i - 1\right\rangle^2} - 1\right). \quad \text{Eq 1}$$

Here $I_{\boldsymbol{C}} = tr(\boldsymbol{C})$ is the first and $IV_{\boldsymbol{C}}^i = \boldsymbol{M}_i \cdot (\boldsymbol{C}\boldsymbol{M}_i)$ is the fourth invariant of the right Cauchy-Green stretch tensor $\boldsymbol{C} = \boldsymbol{F}^T\boldsymbol{F}$ and the structural tensor $\boldsymbol{M}_i \otimes \boldsymbol{M}_i$ that measures square of the stretch along the fiber direction $\boldsymbol{M}_i$ in the reference configuration and is equal to

$$IV_{\boldsymbol{C}}^i = \lambda_z^2 cos^2\gamma^i + \lambda_\theta^2 sin^2\gamma^i,$$

where γ^i is the angle that a fiber family i makes with the longitudinal direction. This constitutive relation phenomenologically accounts for the longitudinally-oriented elastic fibers with γ^i and material parameters c_1^1, c_2^1, passive contributions of circumferential smooth muscle cells (SMCs) with $\gamma^i = 90°$ and material parameters c_1^2, c_2^2, and two families of helical collagen fibers that have the same mechanical properties and are oriented at $\gamma^i = \gamma$ with

material parameters $c_1^3 = c_1^4, c_2^3 = c_2^4$. Macaulay brackets $\langle(\cdot)\rangle = \frac{1}{2}[(\cdot) + |(\cdot)|]$ are used to filter positive values so fibers only contribute to stress during tension.

The total Cauchy stress for an incompressible material (det $\boldsymbol{F} = 1$) can then be calculated as [53]:

$$\boldsymbol{t} = -p\boldsymbol{I} + \bar{\boldsymbol{t}} = -p\boldsymbol{I} + \overbrace{2\frac{\partial W}{\partial I_{\boldsymbol{C}}}\boldsymbol{B} + 2\sum_{i=1}^{4}\frac{\partial W}{\partial IV_{\boldsymbol{C}}^{i}}\boldsymbol{m}_i \otimes \boldsymbol{m}_i}^{\bar{\boldsymbol{t}}}, \quad \text{Eq 2}$$

where, $\boldsymbol{m}_i = \boldsymbol{F}\boldsymbol{M}_i$ is the push-forward of the unit vector $\boldsymbol{M}_i$, p is the Lagrange multiplier, and $\boldsymbol{B} = \boldsymbol{F}\boldsymbol{F}^T$ is the left Cauchy-Green stretch tensor. The constitutive parameters were determined by minimizing the difference between the experimentally-measured Cauchy stresses adjusted for the flattening of the specimens[42], and the theoretical stresses determined using Eq 2. To ensure parameter uniqueness, we have performed a non-parametric bootstrap as described previously[52,54]. It included 2000 iterations of random sampling and fitting, followed by the analysis of the probability distribution of each parameter to determine the global minimum. The coefficient of determination[55] R^2 was used as a measure of the goodness of the fit, and it was greater than 0.91 for all specimens.

Age-group-specific constitutive parameters were determined by generating multi ratio stress-controlled biaxial curves with the steps of 1kPa for all specimens and then finding the median, 25th percentile, and 75th percentile stretches in each age group at each biaxial stress level as described previously[42,52,55,56].

2.5 Kinematics of residual and physiologic states

Arterial morphometry measurements and constitutive parameters were used to determine the residual and physiologic stress-stretch states. The deformation gradients associated with transitions from the *stress-free* to the *load-free* and to the *in vivo loaded* states can be written as[53,57–59] $\boldsymbol{F}_{res} = diag\left[\frac{\partial \rho}{\partial R}, \mathrm{K}\frac{\rho}{R}, \lambda_\zeta\right]$, $\boldsymbol{F}_{load} = diag\left[\frac{\partial r}{\partial \rho}, \frac{r}{\rho}, \lambda_z^{in\ situ}\right]$ and $\boldsymbol{F}_{phys} = \boldsymbol{F}_{load}\boldsymbol{F}_{res} = diag\left[\frac{\partial r}{\partial R}, \frac{r}{R}\mathrm{K}, \lambda_\zeta\lambda_z^{in\ situ}\right]$, where R, ρ and r represent the *stress-free* radially-cut ring, *load free* and *loaded* ring radii, respectively, $\mathrm{K} = \frac{2\pi}{2\pi - \alpha}$ is a measure of the opening angle, and λ_ζ and $\lambda_z^{in\ situ}$ are the residual and *in situ* longitudinal stretches, respectively. Note that λ_ζ accounts for the flattening of the longitudinal strip during the planar biaxial test[42] and $\lambda_z^{in\ situ}$ is considered to be the same for the SFA and PA segments because it was measured for the entire FPA. Assumption of the incompressibility and lack of perivascular tethering, i.e., zero pressure on the outer surface of the artery, and the balance of linear momentum were applied to determine λ_ζ, ρ, r and the Lagrange multiplier p in Eq 2[42,53,55,57–59]. The averaged through-thickness physiologic stress-stretch state was then determined at the luminal pressure of 100 mmHg[42].

In addition, we have calculated the change in elastic energy W from diastole (80 mmHg) to systole (120 mmHg), change in the average circumferential stretch during the cardiac cycle,

$\lambda_\theta^{cardiac} = \frac{r^{sys}}{r^{dias}}$, and the physiologic circumferential stiffness defined as the change in the average circumferential physiologic stress between systole and diastole divided by the change in the average circumferential stretch[42,55]

$$E_\theta = \frac{t_{\theta\theta}^{phys}(sys) - t_{\theta\theta}^{phys}(dias)}{\lambda_\theta^{phys}(sys) - \lambda_\theta^{phys}(dias)}.$$

2.6 Statistical analysis

Pearson correlation coefficient r was used to assess the strength of linear relation between continuous variables and age, with values closer to ±1 demonstrating stronger relations. Statistical significance of the observed correlations was assessed by testing the hypothesis of no correlation (i.e., the null hypothesis) against the alternative hypothesis of nonzero correlation using an independent sample t-test. Since many morphometric and mechanical characteristics did not satisfy the assumption of normal distribution based on skew and kurtosis levels[60] due to extremely small or large values, Wilcoxon Signed Rank (WSR) test was used to compare them. The null hypothesis was that the median difference between the two arterial segments is zero, and the values of $p < 0.05$ were used as a threshold for statistical significance. Where appropriate, results are presented as median ± standard deviation. When discussing young and old subjects, those are defined as ≤20 and >70 years old.

3 RESULTS

3.1 Vascular Disease

Arteries from ≤20-year-old subjects were mostly healthy, and the average disease stage of the SFA was 1.00, and of the PA 1.05±0.05. With age, the PA segment became significantly more diseased than the SFA ($p < 0.01$, Figure 6), and in >60-year-old subjects, PAs had an average disease stage of 4.1±1.1, while the SFAs were rated at 3.8±1.1. Due to these significant differences (Figure 6), the analysis of the morphometry, structure, mechanics, and physiologic characteristics was carried out both with and without taking vascular disease into account.

3.2 Morphometric Analysis

SFA and PA had different thicknesses in the *stress-free*, *load-free*, and *loaded* configurations (Figure 7A,D,G, $p < 0.01$). PA thickened more sharply than SFA with age, and while in young subjects SFA was thicker than the PA (1.26±0.2 vs 1.19±0.2 mm in the *stress-free*, 1.25±0.4 vs 1.18±0.4mm in the *load-free*, and 0.67±0.2 vs 0.65±0.4mm in the *loaded* state), in the old subjects the results were reversed, and the PA was thicker than the SFA (2.2±0.4 vs 1.8±0.5 mm in the *stress-free*, 2.7±0.6 vs 1.8±0.2mm in the *load-free*, and 1.9±0.4 vs 1.6±0.3 mm in the *loaded* state). The differences in thickness between the two segments were primarily attributed to the differences in disease stage because in subjects that had the same degree of vascular pathology in the SFA and PA, there was no statistically significant difference in either *stress-free*, *load-free, or loaded* thickness ($p > 0.1$).

Circumferential and longitudinal opening angles were statistically different between the SFA and the PA (Figure 7B,C, $p < 0.01$), and both increased with age ($p < 0.01$). The increase in the circumferential opening angle α was more sharp for the SFA (96 ± 50° to 193 ± 90°, $r = 0.4$, $p < 0.01$) than for the PA (105 ± 40° to 139 ± 90°, $r = 0.25$, $p < 0.01$), but the longitudinal opening angle β increased similarly in both segments (SFA 139 ± 60° to 306 ± 30°, $r = 0.76$, $p < 0.01$ and PA 133 ± 50° to 320 ± 30°, $r = 0.76$, $p < 0.01$). After controlling for the disease stage, there was no difference in either of the opening angles between the SFA and the PA segments ($p > 0.43$).

SFAs had larger inner and outer radii than the PAs in both *load-free* and the *loaded* states ($p < 0.01$), and both segments widened with age. Inner and outer radii of the SFA widened with age by 60% ($r = 0.38$, $p < 0.01$, 1.5±0.2mm to 2.4±0.5mm) and 58% ($r = 0.50$, $p < 0.01$, 2.6±0.4mm to 4.2±0.4mm) in the *load-free*, and 43% (2.0±0.4mm to 3.0±0.6mm, $p = 0.12$) and 59% ($r = 0.46$, $p < 0.01$, 2.7±0.4mm to 4.4±0.4mm) in the *loaded* state, respectively. Inner and outer radii of the PA increased with age by 27% ($r = 0.24$, $p < 0.01$, 1.5±0.1mm to 1.9±0.4mm) and 61% ($r = 0.53$, $p < 0.01$, 2.6±0.4mm to 4.2±0.6mm) in the *load-free*, and 42% (1.8±0.2mm to 2.6±0.4mm, $p = 0.13$) and 80% ($r = 0.52$, $p < 0.01$ 2.5±0.4mm to 4.5±0.6mm) in the *loaded* state, respectively. In both segments, the outer radii increased with age faster than the inner radii, suggesting a primarily outward thickening. Differences between the SFA and the PA radii remained statistically significant even after controlling for the disease stage ($p < 0.01$).

3.3 Structural Analysis

Changes in structural characteristics are presented in Figure 8. In both SFAs and PAs, elastic fibers in the EEL became more discontinuous with aging ($p < 0.01$), but elastin in the PA was more fragmented than in the SFA ($p < 0.01$) independently of the disease stage. In the SFA, the elastic fiber discontinuity increased from 1.0±0.9 in young to 3±1 in old subjects ($r = 0.30$, $p < 0.01$), and in the PA it increased from 1.5±0.9 to 4±1 ($r = 0.25$, $p < 0.01$). The number of major breaks in the EEL was not statistically different between the SFA and the PA either before ($p = 0.06$) or after ($p = 0.32$) accounting for the disease stage, and it did not change with aging ($p > 0.78$), fluctuating around 1±1 in both arteries.

Tunica intima was, on average, 11% thicker in the PA compared with the SFA ($p < 0.01$). Interestingly, the intimal thickness was on average 21% and 10% larger in the SFA and PA, respectively, when measured using transverse as opposed to longitudinal sections. Intimal thickness in the SFA increased with age from 20±6μm to 212±300μm ($r = 0.4$, $p < 0.01$) as measured on the transverse, and from 20±6μm to 122±50μm ($r = 0.28$, $p < 0.01$) as measured on the longitudinal sections. In the PA, it increased from 22±4μm to 208±300μm ($r = 0.31$, $p < 0.01$) on the transverse, and from 20±10μm to 153±300μm ($r = 0.30$, $p < 0.01$) on the longitudinal sections. As expected, thicker intima of the PA was a result of greater vascular pathology of this segment compared with the SFA. When both arteries were similarly diseased, their intimal layer thickness was not statistically different ($P > 0.26$).

The thickness of the tunica media was not statistically different between the SFA and the PA segments when assessed using conventional transverse sections both before ($p = 0.51$) and after ($p = 0.21$) taking into account the disease stage. When using the longitudinal sections,

SFA and PA medial thickness was statistically different before accounting for the disease stage ($p = 0.04$), but not after ($p = 0.23$). Aging had no effect on the medial thickness of the SFA or PA when measured using the transverse sections (SFA: 620±200μm, $p = 0.30$, PA: 620±200μm, $p = 0.24$), but when assessed longitudinally, tunica media of the SFA increased with age from 475±100μm to 667±100μm ($r = 0.22$, $p = 0.01$), but stayed constant at 630±200μm ($p = 0.14$) in the PA.

Both the total and the EEL elastin density was different in the SFA and PA, and this result was independent of the disease stage ($p < 0.01$) and confirmed on both transverse and longitudinal sections. The total elastin density, measured on the transverse sections, decreased with age from 8±4% to 4±2% ($r = −0.37$, $p < 0.01$) in the SFA, and from 6±4% to 3±1% ($r = −0.42$, $p < 0.01$) in the PA. When assessed using the longitudinal sections, this density decreased from 7±4% to 3±2% ($r = −0.33$, $p < 0.01$) in the SFA, and from 5±3% to 2±2% ($r = −0.20$, $p = 0.03$) in the PA. EEL elastin density followed similar trends. When measured on the transverse sections, it decreased with age from 37±10% to 20±7% ($r = −0.44$, $p < 0.01$) in the SFA, and from 30±10% to 15±4% ($r = −0.48$, $p < 0.01$) in the PA. When measured on the longitudinal sections, this density decreased from 41±20% to 20±10% ($r = −0.31$, $p < 0.01$) in the SFA, and from 38±10% to 21±10% ($r = −0.22$, $p < 0.01$) in the PA.

3.4 Intrinsic Mechanical Properties

Equibiaxial stress-stretch curves representing the median SFA and PA specimens in each decadal age group along with the 25th and 75th percentiles are plotted in Figure 9. Constitutive parameters for the median curves are summarized in Table 2 and Table 3, and the parameters representing the 25th and 75th percentiles are provided in Appendix 6.1.

Both SFAs and PAs stiffened with age, and their stress-stretch responses became more nonlinear. Though in the longitudinal direction, arteries from the youngest age group appear to be less compliant than arteries of 21–30-year-old subjects (Figure 9A,C), this was not statistically significant and likely stems from the relatively small size of these groups and the natural variation in specimens. Since multiple stress-stretch curves representing the different loading ratios were obtained for both the SFA and the PA specimens, their direct comparison is not straightforward and requires a brief discussion. One way to compare the stress-stretch curves for the two arteries is to create a long vector for each subject containing all experimental data points, and then compare arteries for that subject in each direction of stretch. Another way is to combine data from all subjects into a single long vector, and then compare the SFA to the PA for all subjects at once. In both cases, the analysis violates one of the principal assumptions of the Wilcoxon Signed Rank Test that each pair of observations needs to be independent of other observations. To mitigate this issue, we have compared SFAs and PAs independently for each protocol and at each stress level. When following this approach, the analysis demonstrated that the SFA and PA specimens were not different longitudinally ($p > 0.05$) either before or after controlling for their disease stage. In the circumferential direction, the two arteries were also not statistically different ($p > 0.05$) at low stresses (i.e., <20kPa), but at higher stresses, the SFAs were more compliant than the PAs ($p < 0.05$) before controlling for the disease stage. After accounting for the disease, this

statistical significance disappeared ($p > 0.05$), and the two segments were not different in either direction.

3.5 Physiologic Stress-Stretch State

Figure 10 demonstrates changes in the SFA and PA calculated physiologic *in vivo* stresses with age. The two segments had statistically different circumferential and longitudinal physiologic stresses ($p < 0.01$) that decreased with age ($p < 0.01$). The averaged through-thickness circumferential physiologic stress in the SFA was on average 21% higher than in the PA, and it decreased 49% with age (from 39±20kPa to 26±9kPa, $r = -0.41$, $p < 0.01$). In the PA, the circumferential stress decreased 60% with age (from 37±10kPa to 23±5kPa, $r = -0.44$, $p < 0.01$). In the longitudinal direction, physiologic stresses in the SFAs younger than 50 years were 6% higher than in the PAs, but for the subjects older than 50 years, the results were reversed, and the longitudinal stress was 7% higher in the PA compared with the SFA ($p < 0.01$). Longitudinal stresses decreased with age in both segments, 7.5-fold in the SFA (from 113±80kPa to 15±50kPa, $r = -0.54$, $p < 0.01$), and 1.8-fold in the PA (from 115±60kPa to 63±30kPa, $r = -0.38$, $p < 0.01$), following a decrease in the *in situ* longitudinal pre-stretch of the entire FPA from 1.56±0.04 to 1.14±0.07 ($r = -0.54$, $p < 0.01$). The difference in the physiologic stresses in both directions between the SFA and the PA remained statistically significant ($p < 0.01$) even after accounting for the vascular disease.

As demonstrated in Figure 11, SFAs and PAs experienced similar ($p = 0.15$) circumferential stretch as they deformed from diastole to systole (1.04±0.02 in young vs. 1.02±0.01 in old subjects, $r = -0.40$, $p < 0.01$, Figure 11A), but their stored elastic energy during the cardiac cycle was statistically different ($p < 0.01$). In the SFA, ΔW decreased with age 4-fold from 1.4±2kPa to 0.4±0.2kPa ($r = -0.56$, $p < 0.01$) while in PA, it changed 9.1-fold from 2.5±2kPa to 0.3±0.2kPa ($r = -0.59$, $p < 0.01$) (Figure 11B). Circumferential stiffness was also different in the SFAs and PAs ($p < 0.01$, Figure 11C), but it remained relatively constant with age (SFA: 0.7±0.4MPa, $p = 0.24$, and PA: 06±0.4MPa, $p = 0.3$). After accounting for the disease stage, SFAs and PAs were not different ($p > 0.08$) in any of the cardiac cycle measures, including the circumferential cardiac cycle stretch, stored elastic energy, and the circumferential stiffness.

4 DISCUSSION

Lower extremity arterial repairs are notorious for high rates of failure[6–21], and the dynamic biomechanical environment of the lower limb is thought to play an important role by subjecting the FPA to complex mechanical deformations and producing flow abnormalities during limb flexion[22,26–37]. Computational models[27,35,39,40,49] of device-artery interactions have aimed to improve clinical outcomes through optimized device design, but they rely on accurate input data on segmental arterial properties and loading conditions. The FPA is a long artery that smoothly tapers from the larger and more proximal SFA in the upper thigh to the smaller PA behind the knee without major branches or bifurcations[32,61]. Though both segments function in the same biological environment, the PA experiences more severe mechanical deformations during limb flexion[34,36,37,62], and is known to develop more vascular disease compared with the SFA[41]. The goal of our

study was to compare the structural, morphometric, mechanical, and physiologic characteristics in these two FPA segments, and our results demonstrated that they indeed were significantly different; however, most of these differences were due to greater vascular disease in the PA. When the pathology of the SFA and PA was the same, so were the mechanical properties, but not the physiologic characteristics that remained different due to the larger diameter of the more proximal SFA compared with the PA.

Structurally, young healthy SFAs and PAs were very similar. Their adventitia contained diagonally-oriented collagen fibers, EEL had longitudinal elastic fibers, tunica media was rich in circumferentially-oriented SMCs surrounded by collagen, and the internal elastic lamina (IEL) was a sheet (or sometimes a double sheet) of elastin that separated media from intima[43,47]. One structural difference between the two segments that appeared to be independent of age was 30% more elastin in the more proximal SFA compared with the more distal PA. Aging affected both FPA segments, causing them to widen and thicken, but these changes occurred at different rates. The PAs, for example, had a sharper increase in wall thickness due to greater amounts of vascular disease, and although in young healthy subjects the SFAs were 5% thicker than the PAs, in older arteries, the PAs were 28% thicker than the SFAs. The increase in the overall thickness with age was primarily driven by the increases in intimal and adventitial thickness because tunica media thickness remained the same in both arteries. Interestingly, in both segments, the rate of increase in the outer radius was higher than that of the inner radius, consistent with the compensatory dilation mechanism that allows the artery to keep the hemodynamic wall shear and intramural stresses near the homeostatic target[63–71]. More severe disease of the PA was responsible for its thicker wall compared with the SFA, but when the pathology in both segments was similar, there was no variation in thickness along the length of the FPA.

In addition to wall thickening, the constant turnover of the arterial wall constituents during aging creates residual stresses that are thought to reduce stress gradients across the arterial wall[72–74]. These residual stresses are manifested by the opening of the arterial ring into a sector and by the curving of the longitudinal strip intima outward. Though SFAs and PAs had different circumferential and longitudinal opening angles, these differences disappeared after controlling for vascular disease. To understand these results, it is helpful to discuss the mechanism by which residual stresses form in the FPA as they appear to be different for the longitudinal and circumferential directions. Longitudinally, the residual stresses are manifested by the curving of the axial strip with intima pointing outward[45,52], likely due to significant tension generated by the longitudinal elastic fibers in the EEL that are produced and organized primarily during the perinatal period[63,75] and assume significant tension as the artery grows in length. Aging, mechanical deformations during limb flexion, proteolytic destruction, and other disease processes result in degradation and fragmentation of elastin[76], and the release of tension accumulated in the longitudinal EEL fibers, thereby causing the axial strip to assume flatter shapes (i.e., larger opening angles). Interestingly, independent of the pathology, PAs had more discontinuous elastic fibers compared with the SFAs, suggesting a potential influence of limb flexion-induced deformations that are much more severe in this arterial segment[33,34,36,40]. Independent of this fragmentation, we have also observed large breaks that often propagated through the entire thickness of the EEL of both SFAs and PAs, and they appeared to not be affected by age or arterial location.

In older subjects, these larger breaks were bridged by the collagen fibers that may have contributed to the longitudinal stiffening.

Unlike the longitudinal opening angle, the circumferential opening that results from the arterial ring becoming a sector after transection, is likely affected by different factors. In addition to the IEL that is under tension and is likely the reason for the opening to occur with the intimal layer directed inwards, collagen fibers and glycosaminoglycans that accumulate in the tunica intima and the inner part of the tunica media with age, are likely playing important roles. Growth and remodeling of these constituents, in combination with the degradation of the IEL and the release of its tension as a result of aging and vascular disease, results in larger circumferential opening angles. Since healthy SFAs and PAs have a similar structure, their opening angles are affected to a similar degree by aging and vascular disease.

Structural adaptations with age and the increase in pathology resulted in changes in tissue mechanical behavior. It is important to distinguish between the intrinsic mechanical properties and the mechanical characteristics measured at the physiologic state. Latter is usually assessed by the *in vivo* measurements[77–83] that rely on surrogates of arterial stiffness determined using pulse wave velocity or distensibility, but those are limited to the physiologic pressure range, dependent on the residual stresses, and therefore cannot reliably estimate the intrinsic mechanical properties and the physiologic intramural stresses, stretches, and the elastic strain energy. The use of *ex vivo* biaxial testing allows to assess the intrinsic arterial mechanical behavior, and constitutive modeling can be used to accurately calculate stresses and strains that the artery experiences *in vivo*.

In terms of the intrinsic mechanical behavior, both the SFAs and the PAs stiffened with age, and this stiffening was more pronounced in the longitudinal direction for both segments. Young arteries were on average 43% more compliant longitudinally than circumferentially, while older specimens were almost isotropic with both directions stretching on average ~11% at 100kPa equibiaxial stress. Stiffening of human arteries is known to be associated with degradation and fragmentation of elastin, and the accumulation, cross-linking, and reduction in the undulation of collagen[84,85]. This produces a shift in the load-carrying capacity from elastin in the younger specimens to collagen in the older, resulting in the characteristic exponential stiffening of the biaxial stress-stretch curves that was also observed in our study. Though both SFA and PA segments stiffened with age, the PAs were stiffer than the SFAs circumferentially due to more severe vascular pathology, and their respective mechanical properties were summarized for 7 decadal age groups. Nevertheless, after accounting for the differences in vascular disease between the two segments, we found no statistical difference in their mechanical characteristics in either direction, and these results provide important information to computational models of FPA behavior[26].

The determined intrinsic mechanical properties, in combination with the measured morphometry, allowed the assessment of physiologic arterial characteristics and their comparison with the *in vivo* measurements[30,69,86,87]. At physiologic conditions, SFAs were wider than PAs independent of the pathology. They were also more compliant as observed by the higher proportion of the SFA to PA radii in the *loaded* physiologic state

compared with the *load-free* state, which agrees with previous *in vivo* observations[88]. Over the cardiac cycle, both SFA and PA experienced similar circumferential stretch, but due to differences in the mechanical properties, the stored elastic energy and the circumferential physiologic stiffness were different in the two segments. In young subjects, PAs had 75% more elastic energy available for deformation compared with the SFA, while in older subjects, the SFA had 29% more elastic energy than the PA. The greater elastic reserve in young healthy PAs may be required physiologically to accommodate the limb flexion-induced deformations that are more severe in this arterial segment[34,36,37,62]. These mechanical deformations, coupled with the deleterious effects of age and risk factors, result in greater vascular pathology in the PA compared with the SFA, and therefore diminish the elastic reserve of this artery at a greater rate. Reduction of the elastic reserve as a result of the intrinsic stiffening of the arterial wall can lead to a diminished energy reserve for adaptive remodeling[43], more pronounced bends, higher intramural stress concentrations, and more complex flow patterns in the flexed limb due to the reduction in the ability of the artery to accommodate limb flexion-induced deformations[26], as well as the increase in peripheral vascular resistance[89] which may all contribute to the development and progression of vascular pathology. Interestingly, despite the decreasing physiologic stresses, cardiac cycle stretch, and stored elastic energy, the circumferential physiologic stiffness remained relatively unchanged with age in both arterial segments, suggesting that E_θ could be used as a measure for long-term arterial homeostasis[64,90,91]. It is important to distinguish this stiffness from the one measured experimentally using the planar biaxial (Figure 9) or inflationextension testing because this metric incorporates longitudinal *in situ* pre-stretch and the residual stresses, and measures the change in stiffness during the cardiac cycle, but not from the zero-stress state.

Unlike the differences in the cardiac cycle measures that were the result of greater vascular disease in the PA segment, the physiologic stress-stretch response remained distinct in the SFA and PA even after controlling for the disease stage. In both segments, the physiologic stresses reduced with age, and the reduction was faster longitudinally than circumferentially – the observation that was described previously in human SFAs[42]. SFAs also had 21% higher circumferential stresses than the PAs[47], and the reduction of circumferential wall stress with more distal FPA location was reported previously using *in vivo* methods[69]. Importantly, even after accounting for the vascular disease, the physiologic stress-stretch state of the SFA and PA remained statistically different, likely due to different arterial geometry.

While these data improve our understanding of mechanophysiology of the lower limb arteries, the study needs to be considered in the context of its limitations. First, the goal of this study was to assess regional differences in the mechanical properties along the FPA length independent of vascular disease. This is not the same as determining the effects of vascular disease on the mechanical properties. Though both are important questions, they require different approaches. To evaluate how the mechanical properties change along the length of the artery, it is important to be consistent with the anatomical locations where the SFAs and PAs are sampled across all subjects. To answer the second question, one needs to sample from multiple locations with different disease severities that could vary subject-to-subject. While our current study focused on answering the first question, further studies to

investigate the effects of vascular disease of mechanics, structure, and function of lower extremity arteries are warranted.

Second, the arterial wall was assumed homogeneous, while it clearly consists of distinctly different intimal, medial, and adventitial layers. While many studies attempt to separate arterial layers and test them individually[92–94], the atraumatic separation is extremely challenging (if at all possible) in healthy young FPAs. Additionally, layer separation disturbs the integrity of the arterial wall, questioning if the sum of the individual layer responses actually equals the behavior of the whole. This is particularly important to remember if the ultimate goal of these data is the calculation of intramural stress-stretch responses in computational models of device-artery interactions, because these models often focus on the average or maximum stresses in the arterial wall.

Third, arteries were assumed to be axisymmetric, which is a reasonable assumption for young healthy arteries, but is a clear simplification for diseased specimens that may have non-symmetric and highly nonuniform pathologies. While the incorporation of complex arterial geometries can be done using imaging and computational simulations, it is less clear how to determine the mechanical characteristics of individual plaque components without disturbing the integrity of the tissue. Fourth, mechanical testing was performed in a quasistatic manner, and the constitutive modeling did not account for the viscoelastic effects. Dynamic testing and tissue viscoelasticity may have significant effects on the reported mechanical behavior and warrant further investigation.

Fifth, since the blood pressure information was not available from the deceased human donors, we have used normal values of blood pressure for all subjects, independent of their age. Hypertension is known to be more prevalent in the older population, but if it is controlled by medication, the values of pressure are expected to be normal. Nevertheless, the reported mechanical and morphometric properties, along with the detailed framework, allows one to calculate the physiologic stress-stretch state for any blood pressure if so desired, but we do not expect this to change the results of our comparison, as higher blood pressure would equally affect both the SFA and the PA segments.

Sixth, the presented analysis neglects the effects of perivascular tethering on the outer surface of the FPA wall, which may affect the assessment of physiologic stress-stretch behavior. Perivascular tethering in the arteries of the lower limb is not well characterized, and more experiments are needed to quantify it [95]. Seventh, our analysis did not consider the active SMC responses, while the FPA is a muscular artery, and most of its tunica media is occupied by SMCs. Changes in SMC function with age and disease are well-recognized[96–98], but unfortunately cannot be reliably measured in specimens from deceased human donors. For this reason, we have not included this characterization in our analysis and have focused on passive mechanical properties. Fortunately, many constitutive relations that describe active and passive behavior of arteries[53,99,100] mix the two components in an additive fashion, which simplifies supplementation of our passive data with active SMC characteristics when comprehensive human data become available.

Finally, our analysis neglects the effects of gender and risk factors that are likely responsible for the appreciable variation in morphometry, structure, and mechanical properties[101]. While our current sample size did not allow us to perform this analysis while also controlling for age and disease, we hope that these studies will be done in the future. While these limitations exist, it is important to remember that they likely affect both the SFA and the PA segments similarly, and therefore are unlikely to drastically change our conclusions.

5 CONCLUSIONS

The morphometric, structural, mechanical, and physiologic characteristics of the SFA and PA that comprise the FPA in the lower extremity are distinctly different, but mostly due to worse vascular disease in the PA. When the two arteries are equally diseased or are both healthy, the mechanical properties are similar, but the physiologic characteristics remain different due to differences in vessel size. These data help better understand the mechanophysiology of the lower extremity arteries, inform computational models of their repair, and may guide the development of materials and devices to improve PAD treatments.

ACKNOWLEDGEMENTS

This work was supported by NHLBI HL125736 and HL147128. The authors also wish to acknowledge Live On Nebraska for their help and support, and thank tissue donors and their families for making this study possible.

6: APPENDIX

6.1 Variability of mechanical properties within age groups

The four-fiber family model constitutive parameters representing the 25th and 75th percentiles within each age group for the SFAs are summarized in Table 4 and Table 5, and for the PAs they are provided in Table 6 and Table 7.

Table 4:

Parameters of the four-fiber family constitutive model describing the 25th percentile response of human SFAs in 7 age groups. A total of 19 different loading protocols were used to determine the constitutive parameters for this model. The coefficient of determination $R^2 \geq 0.99$ for all age groups.

Age group (years)	C_{gr}, kPa	C_1^1, kPa	C_2^1	C_1^2, kPa	C_2^2	$C_3^2 = C_4^2$, kPa	$C_3^2 = C_4^2$	γ°
16±2 (12–20)	11.34	21.84	0.40	0.14	10.83	9.36	2.69	66.62
26±4 (21–30)	14.37	13.06	0.76	1.68	7.70	2.86	6.43	66.31
37±2 (31–40)	0.09	28.77	0.66	1.40	15.90	32.41	0.93	60.80
46±3 (41–50)	19.56	15.41	3.74	25.81	19.31	1.89	22.77	51.82
57±3 (51–60)	29.85	0.55	22.87	13.38	41.68	1.05	54.94	46.84
64±3 (61–70)	0.06	39.48	10.11	8.50	68.40	52.19	20.34	53.57
76±7 (71–92)	24.46	50.80	31.42	44.55	60.75	8.59	111.64	40.67

Table 5:

Parameters of the four-fiber family constitutive model describing the 75th percentile response of human SFAs in 7 age groups. A total of 19 different loading protocols were used to determine the constitutive parameters for this model. The coefficient of determination $R^2 \geq 0.99$ for all age groups.

Age group (years)	C_{gr}, kPa	C_1^1, kPa	C_2^1	C_1^2, kPa	C_2^2	$C_3^2 = C_4^2$, kPa	$C_3^2 = C_4^2$	γ°
16±2 (12–20)	0.62	17.17	0.23	10.78	0.55	4.92	0.83	51.72
26±4 (21–30)	5.39	6.64	0.44	3.12	2.90	1.41	2.69	56.06
37±2 (31–40)	5.23	15.30	0.73	0.10	0.08	5.26	5.39	71.35
46±3 (41–50)	6.24	10.05	0.81	10.29	6.29	1.99	6.07	56.79
57±3 (51–60)	0.01	11.14	2.63	5.35	7.79	15.77	2.45	53.27
64±3 (61–70)	4.18	16.28	3.68	7.09	7.65	1.30	13.88	46.66
76±7 (71–92)	2.18	21.53	5.49	11.80	6.92	1.11	26.25	42.96

Table 6:

Parameters of the four-fiber family constitutive model describing the 25th percentile response of human PAs in 7 age groups. A total of 19 different loading protocols were used to determine the constitutive parameters in this model. The coefficient of determination $R^2 \geq 0.99$ for all age groups.

Age group (years)	C_{gr}, kPa	C_1^1, kPa	C_2^1	C_1^2, kPa	C_2^2	$C_3^2 = C_4^2$, kPa	$C_3^2 = C_4^2$	γ°
16±2 (12–20)	7.02	26.84	0.30	0.22	9.52	12.69	3.75	67.25
26±4 (21–30)	13.20	5.16	0.87	7.41	7.94	0.13	12.65	58.32
37±2 (31–40)	17.13	2.20	6.67	10.36	24.68	3.70	21.40	60.81
46±3 (41–50)	0.09	0.14	3.46	9.64	30.57	41.17	3.47	33.55
57±3 (51–60)	0.01	46.16	6.94	56.70	47.68	28.27	28.91	53.52
64±3 (61–70)	32.47	13.30	25.61	30.40	36.54	0.39	126.52	47.68
76±7 (71–92)	0.00	111.55	63.11	71.18	80.59	90.67	155.09	54.48

Table 7:

Parameters of the four-fiber family constitutive model describing the 75th percentile response of human PAs in 7 age groups. A total of 19 different loading protocols were used to determine the constitutive parameters in this model. The coefficient of determination $R^2 \geq 0.99$ for all age groups.

Age group (years)	C_{gr}, kPa	C_1^1, kPa	C_2^1	C_1^2, kPa	C_2^2	$C_3^2 = C_4^2$, kPa	$C_3^2 = C_4^2$	γ°
16±2 (12–20)	0.03	19.78	0.19	0.10	8.78	17.85	0.83	66.92
26±4 (21–30)	0.01	10.98	0.08	0.02	9.36	6.06	1.97	69.68
37±2 (31–40)	0.03	24.54	0.19	5.42	7.54	16.69	0.04	63.40

Age group (years)	C_{gr}, kPa	C_1^1, kPa	C_2^1	C_1^2, kPa	C_2^2	$C_3^2 = C_4^2$, kPa	$C_3^2 = C_4^2$	γ°
46±3 (41–50)	6.71	7.40	1.78	13.42	2.59	1.24	6.45	48.83
57±3 (51–60)	1.99	15.26	1.99	2.41	11.71	6.72	6.86	52.15
64±3 (61–70)	1.07	8.66	5.35	12.23	3.34	0.77	15.33	42.94
76±7 (71–92)	0.00	76.59	12.12	25.43	7.21	2.50	32.95	54.90

7 REFERENCES

[1]. Kullo IJ, Rooke TW, Peripheral Artery Disease, N. Engl. J. Med 374 (2016) 861–871. 10.1056/NEJMcp1507631. [PubMed: 26962905]

[2]. Peach G, Griffin M, Jones KG, Thompson MM, Hinchliffe RJ, Diagnosis and management of peripheral arterial disease, BMJ. (2012).

[3]. Boyko EJ, Monteiro-Soares M, Wheeler SGB, Chapter 20: Peripheral Arterial Disease, Foot Ulcers, Lower Extremity Amputations, and Diabetes, n.d.

[4]. Ouriel K, Peripheral arterial disease, Lancet. 358 (2001) 1257–1264. [PubMed: 11675083]

[5]. Mahoney EM, Wang K, Keo HH, Duval S, Smolderen KG, Cohen DJ, Steg G, Bhatt DL, Hirsch AT, Vascular hospitalization rates and costs in patients with peripheral artery disease in the United States., Circ. Cardiovasc. Qual. Outcomes. 3 (2010) 642–51. 10.1161/CIRCOUTCOMES.109.930735. [PubMed: 20940249]

[6]. Adam DJ, Beard JD, Cleveland T, Bell J, Bradbury a W., Forbes JF, Fowkes FGR, Gillepsie I, Ruckley CV, Raab G, Storkey H, Bypass versus angioplasty in severe ischaemia of the leg (BASIL): multicentre, randomised controlled trial., Lancet. 366 (2005) 1925–34. 10.1016/S0140-6736(05)67704-5. [PubMed: 16325694]

[7]. Conte MS, Bandyk DF, Clowes AW, Moneta GL, Seely L, Lorenz TJ, Namini H, Hamdan AD, Roddy SP, Belkin M, Berceli S. a., DeMasi RJ, Samson RH, Berman SS, Results of PREVENT III: a multicenter, randomized trial of edifoligide for the prevention of vein graft failure in lower extremity bypass surgery., J. Vasc. Surg 43 (2006) 742–751. 10.1016/j.jvs.2005.12.058. [PubMed: 16616230]

[8]. Hiramoto JS, Teraa M, De Borst GJ, Conte MS, Interventions for lower extremity peripheral artery disease, Nat. Rev. Cardiol 15 (2018) 332–350. 10.1038/s41569-018-0005-0. [PubMed: 29679023]

[9]. Katsanos K, Spiliopoulos S, Kitrou P, Krokidis M, Karnabatidis D, Risk of death following application of paclitaxel-coated balloons and stents in the femoropopliteal artery of the leg: A systematic review and meta-analysis of randomized controlled trials, J. Am. Heart Assoc 7 (2018). 10.1161/JAHA.118.011245.

[10]. Mills JL, Conte MS, Murad MH, Critical review and evidence implications of paclitaxel drug-eluting balloons and stents in peripheral artery disease, J. Vasc. Surg 70 (2019) 3–7. 10.1016/j.jvs.2019.05.002. [PubMed: 31230649]

[11]. Shishehbor MH, Jaff MR, Percutaneous Therapies for Peripheral Artery Disease, Circulation. 134 (2016) 2008–2027. 10.1161/CIRCULATIONAHA.116.022546. [PubMed: 27956404]

[12]. Scheinert D, Scheinert S, Sax J, Piorkowski C, Bräunlich S, Ulrich M, Biamino G, Schmidt A, Prevalence and clinical impact of stent fractures after femoropopliteal stenting, J. Am. Coll. Cardiol 45 (2005) 312–315. 10.1016/j.jacc.2004.11.026. [PubMed: 15653033]

[13]. Chang CH, Lin JW, Hsu J, Wu LC, Lai MS, Stent revascularization versus bypass surgery for peripheral artery disease in type 2 diabetic patients-an instrumental variable analysis, Sci. Rep 6 (2016) 1–13. 10.1038/srep37177. [PubMed: 28442746]

[14]. Schillinger M, Sabeti S, Loewe C, Dick P, Amighi J, Mlekusch W, Schlager O, Cejna M, Lammer J, Minar E, Balloon angioplasty versus implantation of nitinol stents in the superficial femoral artery., N. Engl. J. Med 354 (2006) 1879–88. 10.1056/NEJMoa051303. [PubMed: 16672699]

[15]. Schillinger M, Sabeti S, Dick P, Amighi J, Mlekusch W, Schlager O, Loewe C, Cejna M, Lammer J, Minar E, Sustained benefit at 2 years of primary femoropopliteal stenting compared with balloon angioplasty with optional stenting., Circulation. 115 (2007) 2745–9. 10.1161/CIRCULATIONAHA.107.688341. [PubMed: 17502568]

[16]. Stavroulakis K, Torsello G, Manal A, Schwindt A, Hericks C, Stachmann A, Schönefeld E, Bisdas T, Results of primary stent therapy for femoropopliteal peripheral arterial disease at 7 years, J. Vasc. Surg 64 (2016) 1696–1702. 10.1016/j.jvs.2016.05.073. [PubMed: 27575816]

[17]. Laird JR, Yeo KK, The Treatment of Femoropopliteal In-Stent Restenosis Back to the Future*, (2012). 10.1016/j.jacc.2011.09.037.

[18]. Qato K, Conway AM, Mondry L, Giangola G, Carroccio A, Management of isolated femoropopliteal in-stent restenosis, J. Vasc. Surg 68 (2018) 807–810. 10.1016/j.jvs.2018.01.030. [PubMed: 30144908]

[19]. Lundgren F, External support of a polytetrafluoroethylene graft improves patency for bypass to below-knee arteries, Ann. Vasc. Surg 27 (2013) 1124–1133. 10.1016/j.avsg.2013.02.009. [PubMed: 23972437]

[20]. Siracuse JJ, a Giles K, Pomposelli FB, Hamdan AD, Wyers MC, Chaikof EL, Nedeau AE, Schermerhorn ML, Results for primary bypass versus primary angioplasty/stent for intermittent claudication due to superficial femoral artery occlusive disease., J. Vasc. Surg 55 (2012) 1001–7. 10.1016/j.jvs.2011.10.128. [PubMed: 22301210]

[21]. Thukkani AK, Kinlay S, Endovascular Intervention for Peripheral Artery Disease, Circ. Res 116 (2015) 1599–1613. 10.1161/CIRCRESAHA.116.303503. [PubMed: 25908731]

[22]. Padilla J, Fadel PJ, Prolonged sitting leg vasculopathy: contributing factors and clinical implications, Am. J. Physiol. - Hear. Circ. Physiol 65211 (2017) ajpheart.00326.2017 10.1152/ajpheart.00326.2017.

[23]. Young C, Deo S, Padilla J, Laughlin MH, Fadel PJ, Pro-atherogenic shear rate patterns in the femoral artery of healthy older adults, Atherosclerosis. 211 (2010) 390–392. 10.1016/j.atherosclerosis.2010.03.017.Pro-atherogenic. [PubMed: 20394928]

[24]. Parker B, Age and flow-mediated dilation: a comparison of dilatory responsiveness in the brachial and popliteal arteries, Am. J. Physiol. Hear. Circ. Physiol 6900 (2006) 3043–3049. 10.1152/ajpheart.00190.2006.

[25]. Newcomer SC, Sauder CL, Kuipers NT, Laughlin MH, a Ray C, Effects of posture on shear rates in human brachial and superficial femoral arteries., Am. J. Physiol. Heart Circ. Physiol 294 (2008) H1833–9. 10.1152/ajpheart.01108.2007. [PubMed: 18245564]

[26]. Desyatova A, Mactaggart J, Romarowski R, Poulson W, Conti M, Kamenskiy A, Effect of aging on mechanical stresses, deformations, and hemodynamics in human femoropopliteal artery due to limb flexion, Biomech. Model. Mechanobiol 17 (2018). 10.1007/s10237-017-0953-z.

[27]. Colombo M, Luraghi G, Cestariolo L, Ravasi M, Airoldi A, Chiastra C, Pennati G, Impact of lower limb movement on the hemodynamics of femoropopliteal arteries: A computational study, Med. Eng. Phys 81 (2020) 105–117. 10.1016/j.medengphy.2020.05.004. [PubMed: 32505663]

[28]. Gökgöl C, Diehm N, Kara L, Büchler P, Quantification of popliteal artery deformation during leg flexion in subjects with peripheral artery disease: a pilot study., J. Endovasc. Ther 20 (2013) 828–35. 10.1583/13-4332MR.1. [PubMed: 24325701]

[29]. Klein AJ, Casserly IP, Messenger JC, Carroll JD, Chen S-YJ, In vivo 3D modeling of the femoropopliteal artery in human subjects based on x-ray angiography: Methodology and validation, Med. Phys 36 (2009) 289–310. 10.1118/1.3006195. [PubMed: 19291969]

[30]. Spinella G, Finotello A, Pane B, Salsano G, Mambrini S, Kamenskiy A, Gazzola V, Cittadini G, Auricchio F, Palombo D, Conti M, In Vivo Morphological Changes of the Femoropopliteal Arteries due to Knee Flexion After Endovascular Treatment of Popliteal Aneurysm., J. Endovasc. Ther 26 (2019) 496–504. 10.1177/1526602819855441. [PubMed: 31198084]

[31]. Maleckis K, Anttila E, Aylward P, Poulson W, Desyatova A, MacTaggart J, Kamenskiy A, Nitinol Stents in the Femoropopliteal Artery: A Mechanical Perspective on Material, Design, and Performance., Ann. Biomed. Eng (2018). 10.1007/s10439-018-1990-1.

[32]. Ansari F, Pack LK, Brooks SS, Morrison TM, Design considerations for studies of the biomechanical environment of the femoropopliteal arteries, J. Vasc. Surg 58 (2013) 804–813. 10.1016/j.jvs.2013.03.052. [PubMed: 23870198]

[33]. MacTaggart JN, Phillips NY, Lomneth CS, Pipinos III, Bowen R, Timothy Baxter B, Johanning J, Matthew Longo G, Desyatova AS, Moulton MJ, Dzenis YA, Kamenskiy AV, Three-dimensional bending, torsion and axial compression of the femoropopliteal artery during limb flexion, J. Biomech 47 (2014) 2249–2256. 10.1016/j.jbiomech.2014.04.053. [PubMed: 24856888]

[34]. Desyatova A, Poulson W, Deegan P, Lomneth C, Seas A, Maleckis K, MacTaggart J, Kamenskiy A, Limb flexion-induced twist and associated intramural stresses in the human femoropopliteal artery, J. R. Soc. Interface. 14 (2017) 20170025 10.1098/rsif.2017.0025. [PubMed: 28330991]

[35]. Desyatova A, Poulson W, MacTaggart J, Maleckis K, Kamenskiy A, Cross-sectional pinching in human femoropopliteal arteries due to limb flexion, and stent design optimization for maximum cross-sectional opening and minimum intramural stresses., J. R. Soc. Interface. 15 (2018) 10–14. 10.1098/rsif.2018.0475.

[36]. Poulson W, Kamenskiy A, Seas A, Deegan P, Lomneth C, MacTaggart J, Limb flexion-induced axial compression and bending in human femoropopliteal artery segments, J. Vasc. Surg 67 (2018) 607–613. 10.1016/j.jvs.2017.01.071. [PubMed: 28526560]

[37]. Cheng CP, Choi G, Herfkens RJ, Taylor CA, The Effect of Aging on Deformations of the Superficial Femoral Artery Resulting from Hip and Knee Flexion: Potential Clinical Implications, J. Vasc. Interv. Radiol 21 (2010) 195–202. 10.1016/j.jvir.2009.08.027. [PubMed: 20022767]

[38]. Scheinert D, Treatment Paradigms for the Superficial Femoral Artery Are They A-Changin?*, 2012 10.1016/j.jcin.2012.01.003.

[39]. Maleckis K, Deegan P, Poulson W, Sievers C, Desyatova A, MacTaggart J, Kamenskiy A, Comparison of femoropopliteal artery stents under axial and radial compression, axial tension, bending, and torsion deformations., J. Mech. Behav. Biomed. Mater 75 (2017) 160–168. 10.1016/j.jmbbm.2017.07.017. [PubMed: 28734257]

[40]. MacTaggart J, Poulson W, Seas A, Deegan P, Lomneth C, Desyatova A, Maleckis K, Kamenskiy A, Stent Design Affects Femoropopliteal Artery Deformation., Ann. Surg (2018) 1 10.1097/SLA.0000000000002747.

[41]. Watt J, Origin of femoro-popliteal occlusions., Br. Med. J 2 (1965) 1455–1459. [PubMed: 5849435]

[42]. Jadidi M, Desyatova A, MacTaggart J, Kamenskiy A, Mechanical stresses associated with flattening of human femoropopliteal artery specimens during planar biaxial testing and their effects on the calculated physiologic stress-stretch state., Biomech. Model. Mechanobiol 18 (2019) 1591–1605. 10.1007/s10237-019-01162-0. [PubMed: 31069592]

[43]. Kamenskiy A, Seas A, Bowen G, Deegan P, Desyatova A, Bohlim N, Poulson W, Mactaggart J, In situ longitudinal pre-stretch in the human femoropopliteal artery, Acta Biomater 32 (2016) 231–237. 10.1016/j.actbio.2016.01.002. [PubMed: 26766633]

[44]. Kamenskiy A, Poulson W, Sim S, Reilly A, Luo J, Mactaggart J, Prevalence of Calcification in Human Femoropopliteal Arteries and its Association with Demographics, Risk Factors, and Arterial Stiffness., Arterioscler. Thromb. Vasc. Biol 38 (2018) ATVBAHA.117.310490 10.1161/ATVBAHA.117.310490.

[45]. Desyatova A, MacTaggart J, Kamenskiy A, Constitutive modeling of human femoropopliteal artery biaxial stiffening due to aging and diabetes., Acta Biomater 64 (2017) 50–58. 10.1016/j.actbio.2017.09.042. [PubMed: 28974476]

[46]. Jadidi M, Razian SA, Habibnezhad M, Anttila E, Kamenskiy A, Mechanical, structural, and physiologic differences in human elastic and muscular arteries of different ages: Comparison of the descending thoracic aorta to the superficial femoral artery., Acta Biomater (2020). 10.1016/j.actbio.2020.10.035.

[47]. V Kamenskiy A, Pipinos II, Dzenis YA, Phillips NY, Desyatova AS, Kitson J, Bowen R, MacTaggart JN, Effects of age on the physiological and mechanical characteristics of human femoropopliteal arteries., Acta Biomater 11 (2015) 304–13. 10.1016/j.actbio.2014.09.050. [PubMed: 25301303]

[48]. Kamenskiy AV, Pipinos II, Dzenis YA, Lomneth CS, Kazmi S. a J., Phillips NY, MacTaggart JN, Passive biaxial mechanical properties and in vivo axial pre-stretch of the diseased human femoropopliteal and tibial arteries., Acta Biomater 10 (2014) 1301–13. 10.1016/j.actbio.2013.12.027. [PubMed: 24370640]

[49]. Colombo M, Bologna M, Garbey M, Berceli S, He Y, Rodriguez Matas JF, Migliavacca F, Chiastra C, Computing patient-specific hemodynamics in stented femoral artery models obtained from computed tomography using a validated 3D reconstruction method, Med. Eng. Phys 75 (2020) 23–35. 10.1016/j.medengphy.2019.10.005. [PubMed: 31679904]

[50]. Gökgöl C, Diehm N, Räber L, Büchler P, Prediction of restenosis based on hemodynamical markers in revascularized femoro-popliteal arteries during leg flexion, Biomech. Model. Mechanobiol (2019). 10.1007/s10237-019-01183-9.

[51]. Gökgöl C, Diehm N, Nezami FR, Büchler P, Nitinol Stent Oversizing in Patients Undergoing Popliteal Artery Revascularization: A Finite Element Study, Ann. Biomed. Eng 43 (2015) 2868–2880. 10.1007/s10439-015-1358-8. [PubMed: 26101031]

[52]. Kamenskiy A, Seas A, Deegan P, Poulson W, Anttila E, Sim S, Desyatova A, MacTaggart J, Constitutive description of human femoropopliteal artery aging, Biomech. Model. Mechanobiol 16 (2017) 681–692. 10.1007/s10237-016-0845-7. [PubMed: 27771811]

[53]. Holzapfel GA, Ogden RW, Constitutive modelling of arteries, Proc. R. Soc. A Math. Phys. Eng. Sci 466 (2010) 1551–1597. 10.1098/rspa.2010.0058.

[54]. Ferruzzi J, Vorp DA, Humphrey JD, On constitutive descriptors of the biaxial mechanical behaviour of human abdominal aorta and aneurysms., J. R. Soc. Interface. 8 (2011) 435–50. 10.1098/rsif.2010.0299. [PubMed: 20659928]

[55]. Jadidi M, Habibnezhad M, Anttila E, Maleckis K, Desyatova A, MacTaggart J, Kamenskiy A, Mechanical and structural changes in human thoracic aortas with age., Acta Biomater 103 (2020) 172–188. 10.1016/j.actbio.2019.12.024. [PubMed: 31877371]

[56]. Anttila E, Balzani D, Desyatova A, Deegan P, MacTaggart J, Kamenskiy A, Mechanical damage characterization in human femoropopliteal arteries of different ages, Acta Biomater 90 (2019) 225–240. 10.1016/j.actbio.2019.03.053. [PubMed: 30928732]

[57]. Sommer G, Holzapfel GA, 3D constitutive modeling of the biaxial mechanical response of intact and layer-dissected human carotid arteries., J. Mech. Behav. Biomed. Mater 5 (2012) 116–28. 10.1016/j.jmbbm.2011.08.013. [PubMed: 22100086]

[58]. Holzapfel GA, Gasser TC, Ogden RW, O.R. W, A New Constitutive Framework For Arterial Wall Mechanics And A Comparative Study of Material Models, J Elast 61 (2000) 1–48.

[59]. Humphrey JD, Cardiovascular Solid Mechanics, Springer New York, New York, NY, 2002 10.1007/978-0-387-21576-1.

[60]. Posten HO, Robustness of the Two-Sample T-Test, in: Robustness Stat. Methods Nonparametric Stat, Springer Netherlands, 1984: pp. 92–99. 10.1007/978-94-009-6528-7_23.

[61]. Netter F, Colacino S, Atlas of human anatomy, 1989.

[62]. Balkestein EJ, Staessen J. a., Wang J-G, van der Heijden-Spek JJ, Van Bortel LM, Barlassina C, Bianchi G, Brand E, Herrmann S-M, Struijker-Boudier H. a., Carotid and Femoral Artery Stiffness in Relation to Three Candidate Genes in a White Population, Hypertension. 38 (2001) 1190–1197. 10.1161/hy1101.095992. [PubMed: 11711521]

[63]. Humphrey JD, Eberth JF, Dye WW, Gleason RL, Fundamental role of axial stress in compensatory adaptations by arteries., J. Biomech 42 (2009) 1–8. 10.1016/j.jbiomech.2008.11.011. [PubMed: 19070860]

[64]. Humphrey JD, Dufresne ER, Schwartz M. a., Mechanotransduction and extracellular matrix homeostasis, Nat. Rev. Mol. Cell Biol 15 (2014) 802–812. 10.1038/nrm3896. [PubMed: 25355505]

[65]. Varnava AM, Davies MJ, Relation between coronary artery remodelling (compensatory dilatation) and stenosis in human native coronary arteries, Heart 86 (2001) 207–211. 10.1136/heart.86.2.207. [PubMed: 11454845]

[66]. Keren G, Compensatory enlargement, remodeling, and restenosis, Adv. Exp. Med. Biol 430 (1997) 187–196. 10.1007/978-1-4615-5959-7_16. [PubMed: 9330729]

[67]. Stiel GM, Stiel LS, Schofer J, Donath K, Mathey DG, Impact of compensatory enlargement of atherosclerotic coronary arteries on angiographic assessment of coronary artery disease., Circulation. 80 (1989) 1603–1609. 10.1161/01.CIR.80.6.1603. [PubMed: 2598424]

[68]. Glagov S, Weisenberg E, Zarins CK, Stankunavicius R, Kolettis GJ, Compensatory enlargement of human atherosclerotic coronary arteries., N Engl J Med 316 (1987) 1371–1375. [PubMed: 3574413]

[69]. De Basso R, Åstrand H, Ahlgren ÅR, Sandgren T, Länne T, Low wall stress in the popliteal artery: Other mechanisms responsible for the predilection of aneurysmal dilatation?, Vasc. Med. (United Kingdom). 19 (2014) 131–136. 10.1177/1358863X14524851.

[70]. Zarins CK, Zatina MA, Giddens DP, Ku DN, Glagov S, Shear stress regulation of artery lumen diameter in experimental atherogenesis, J. Vasc. Surg 5 (1987) 413–420. 10.1016/0741-5214(87)90048-6. [PubMed: 3509594]

[71]. Humphrey JD, Mechanisms of arterial remodeling in hypertension: coupled roles of wall shear and intramural stress., Hypertension. 52 (2008) 195–200. 10.1161/HYPERTENSIONAHA.107.103440. [PubMed: 18541735]

[72]. Cardamone L, Valent?n A, Eberth JF, Humphrey JD, Origin of axial prestretch and residual stress in arteries., Biomech Model Mechanobiol (2009).

[73]. Taber LA, Humphrey JD, Stress-modulated growth, residual stress, and vascular heterogeneity., J Biomech Eng 123 (2001) 528–535. [PubMed: 11783722]

[74]. Rachev A, Greenwald S, Residual strains in conduit arteries, J. Biomech 36 (2003) 661–670. 10.1016/S0021-9290(02)00444-X. [PubMed: 12694996]

[75]. Mithieux SM, Weiss AS, Elastin., Adv. Protein Chem 70 (2005) 437–61. 10.1016/S0065-3233(05)70013-9. [PubMed: 15837523]

[76]. Duca L, Blaise S, Romier B, Laffargue M, Gayral S, El Btaouri H, Kawecki C, Guillot A, Martiny L, Debelle L, Maurice P, Matrix ageing and vascular impacts: focus on elastin fragmentation, Cardiovasc. Res 110 (2016) 298–308. 10.1093/cvr/cvw061. [PubMed: 27009176]

[77]. Boutouyrie P, Laurent S, Benetos A, Girerd XJ, Hoekst APG, Safar ME, Opposing effects of ageing on distal and proximal large arteries in hypertensives, J. Hypertens 10 (1992) S87–S92. 10.1097/00004872-199208001-00023.

[78]. Bortolotto LA, Hanon O, Franconi G, Boutouyrie P, Legrain S, Girerd X, The aging process modifies the distensibility of elastic but not muscular arteries, Hypertension. 34 (1999) 889–892. 10.1161/01.hyp.34.4.889. [PubMed: 10523379]

[79]. Van Der Heijden-Spek JJ, Staessen JA, Fagard RH, Hoeks AP, Struijker Boudier HA, Van Bortel LM, Effect of age on brachial artery wall properties differs from the aorta and is gender dependent: A population study, Hypertension. 35 (2000) 637–642. 10.1161/01.HYP.35.2.637. [PubMed: 10679510]

[80]. Mourad J-J, Girerd X, Boutouyrie P, Safar M, Laurent S, Opposite Effects of Remodeling and Hypertrophy on Arterial Compliance in Hypertension, Hypertension. 31 (1998) 529–533. 10.1161/01.HYP.31.1.529. [PubMed: 9453357]

[81]. Ruitenbeek AG, Van Der Cammen TJM, Van Den Meiracker AH, Mattace-Raso FUS, Age and blood pressure levels modify the functional properties of central but not peripheral arteries, Angiology. 59 (2008) 290–295. 10.1177/0003319707305692. [PubMed: 18388084]

[82]. Zhang Y, Agnoletti D, Protogerou AD, Topouchian J, Wang J-G, Xu Y, Blacher J, Safar ME, Characteristics of pulse wave velocity in elastic and muscular arteries, J. Hypertens 31 (2013) 554–559. 10.1097/HJH.0b013e32835d4aec. [PubMed: 23615212]

[83]. Kamenskiy A, Miserlis D, Adamson P, Adamson M, Knowles T, Neme J, Koutakis P, Phillips N, Pipinos I, MacTaggart J, Patient demographics and cardiovascular risk factors differentially influence geometric remodeling of the aorta compared with the peripheral arteries., Surgery. 158 (2015) 1617–1627. 10.1016/j.surg.2015.05.013. [PubMed: 26096560]

[84]. Rezakhaniha R, · Agianniotis A, · Schrauwen JTC, · Griffa A, · Sage D, · Bouten CVC, · Van De Vosse FN, · Unser M, · Stergiopulos N, Schrauwen JTC, Griffa A, Sage D, Bouten CVC, Agianniotis A, Experimental investigation of collagen waviness and orientation in the arterial adventitia using confocal laser scanning microscopy, Biomech Model Mechanobiol 11 (2012) 461–473. 10.1007/s10237-011-0325-z. [PubMed: 21744269]

[85]. Tsamis A, Krawiec JT, a Vorp D, Elastin and collagen fibre microstructure of the human aorta in ageing and disease: a review., J. R. Soc. Interface. 10 (2013) 20121004 10.1098/rsif.2012.1004. [PubMed: 23536538]

[86]. Sandgren T, Sonesson B, Ahlgren a. R., Lanne T, Factors predicting the diameter of the popliteal artery in healthy humans, J. Vasc. Surg 28 (1998) 284–289. 10.1016/S0741-5214(98)70164-8. [PubMed: 9719323]

[87]. Debasso R, Åstrand H, Bjarnegård N, Ahlgren ÅR, Sandgren T, Länne T, The popliteal artery, an unusual muscular artery with wall properties similar to the aorta: Implications for susceptibility to aneurysm formation?, J. Vasc. Surg 39 (2004) 836–842. 10.1016/j.jvs.2003.12.005. [PubMed: 15071452]

[88]. Tai NR, a Giudiceandrea, Salacinski HJ, Seifalian a M., Hamilton G, In vivo femoropopliteal arterial wall compliance in subjects with and without lower limb vascular disease., J. Vasc. Surg 30 (1999) 936–45. [PubMed: 10550193]

[89]. Amery A, Wasir H, Bulpitt C, Conway J, Fagard R, Lijnen P, Reybrouck T, Aging and the cardiovascular system., Acta Cardiol 33 (1978) 443–67. [PubMed: 375649]

[90]. Humphrey JD, Vascular adaptation and mechanical homeostasis at tissue, cellular, and sub-cellular levels., Cell Biochem. Biophys 50 (2008) 53–78. 10.1007/s12013-007-9002-3. [PubMed: 18209957]

[91]. Ferruzzi J, Madziva D, Caulk AW, Tellides G, Humphrey JD, Compromised mechanical homeostasis in arterial aging and associated cardiovascular consequences., Biomech. Model. Mechanobiol 17 (2018) 1281–1295. 10.1007/s10237-018-1026-7. [PubMed: 29754316]

[92]. Sommer G, Regitnig P, Koltringer L, Holzapfel GA, Biaxial mechanical properties of intact and layer-dissected human carotid arteries at physiological and supra-physiological loadings., Am J Physiol Hear. Circ Physiol 298 (2010) H898–912.

[93]. Amabili M, Balasubramanian P, Bozzo I, Breslavsky ID, Ferrari G, Layer-specific hyperelastic and viscoelastic characterization of human descending thoracic aortas, J. Mech. Behav. Biomed. Mater 99 (2019) 27–46. 10.1016/j.jmbbm.2019.07.008. [PubMed: 31330442]

[94]. Holzapfel GA, Sommer G, Auer M, Regitnig P, Ogden RW, Layer-specific 3D residual deformations of human aortas with non-atherosclerotic intimal thickening., Ann Biomed Eng 35 (2007) 530–545. [PubMed: 17285364]

[95]. Ferruzzi J, Di Achille P, Tellides G, Humphrey JD, Di Achille P, Tellides G, Humphrey JD, Combining in vivo and in vitro biomechanical data reveals key roles of perivascular tethering in central artery function, PLoS One 13 (2018) e0201379. [PubMed: 30192758]

[96]. Montero D, Pierce GL, Stehouwer CDA, Padilla J, Thijssen DHJ, The impact of age on vascular smooth muscle function in humans., J. Hypertens 33 (2015) 445–53; discussion 453. 10.1097/HJH.0000000000000446. [PubMed: 25479030]

[97]. Seawright JW, Sreenivasappa H, Gibbs HC, Padgham S, Shin SY, Chaponnier C, Yeh AT, Trzeciakowski JP, Woodman CR, Trache A, Vascular Smooth Muscle Contractile Function Declines With Age in Skeletal Muscle Feed Arteries, Front. Physiol 9 (2018) 1–12. 10.3389/fphys.2018.00856. [PubMed: 29377031]

[98]. Lacolley P, Regnault V, Avolio AP, Smooth muscle cell and arterial aging: Basic and clinical aspects, Cardiovasc. Res 114 (2018) 513–528. 10.1093/cvr/cvy009. [PubMed: 29514201]

[99]. Wagner HP, Humphrey JD, Differential passive and active biaxial mechanical behaviors of muscular and elastic arteries: basilar versus common carotid., J. Biomech. Eng 133 (2011) 051009 10.1115/1.4003873. [PubMed: 21599100]

[100]. Rachev A, A Model of Arterial Adaptation to Alterations in Blood Flow, 2000.

[101]. Berenson GS, Srinivasan SR, Bao W, Newman WP, Tracy RE, Wattigney WA, Association between multiple cardiovascular risk factors and atherosclerosis in children and young adults. The Bogalusa Heart Study, N. Engl. J. Med 338 (1998) 1650–1656. 10.1056/NEJM199806043382302. [PubMed: 9614255]

Statement of significance

The femoropopliteal artery (FPA) in the lower limb consists of the superficial femoral (SFA) and popliteal (PA) arteries that are differentially affected by vascular disease. We compared SFAs and PAs from 125 human subjects 13–92 years old using biaxial mechanical testing, constitutive modeling, and bidirectional histology. Our results demonstrate that the two arterial segments are distinctly different, but mostly due to worse vascular disease in the PA. When the two arteries are equally diseased or healthy, the mechanical properties are similar, but the physiologic characteristics remain different. These data help understand the mechanophysiology of the lower extremity arteries, inform computational models of their repair, and may guide the development of materials and devices for peripheral arterial disease treatment.

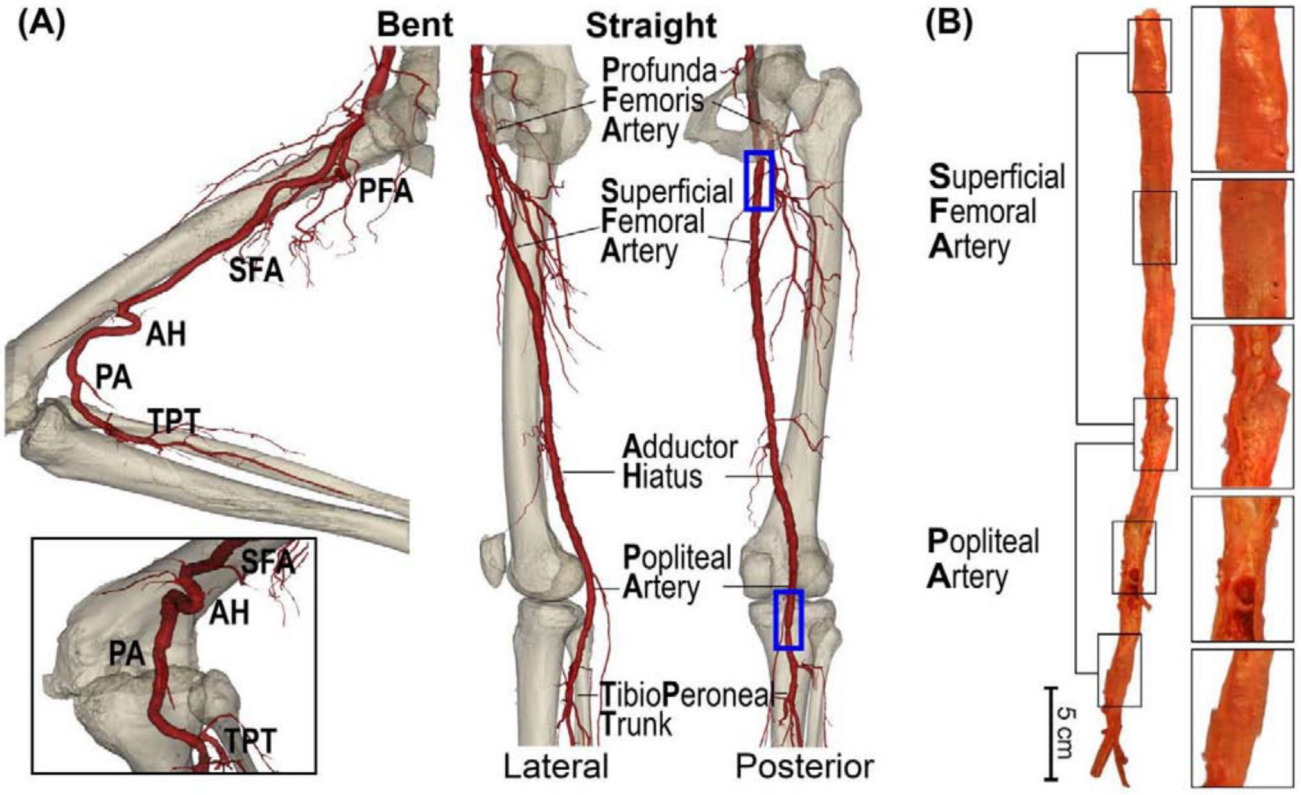

Figure 1:

(A) Anatomy of the femoropopliteal artery (FPA) in the straight (right) and bent (left) limb posture. The FPA is typically divided into the superficial femoral artery (SFA) and the popliteal artery (PA) at the level of the adductor hiatus (AH). The SFA starts at the take off of the profunda femoris artery (PFA) in the upper thigh, and the PA ends at the tibioperoneal trunk (TPT). Note that the artery at the adductor hiatus and behind the knee is experiencing severe deformations during limb flexion. (B) A representative image of the longitudinally-opened 79-year-old male femoropopliteal artery demonstrating SFA and PA segments.

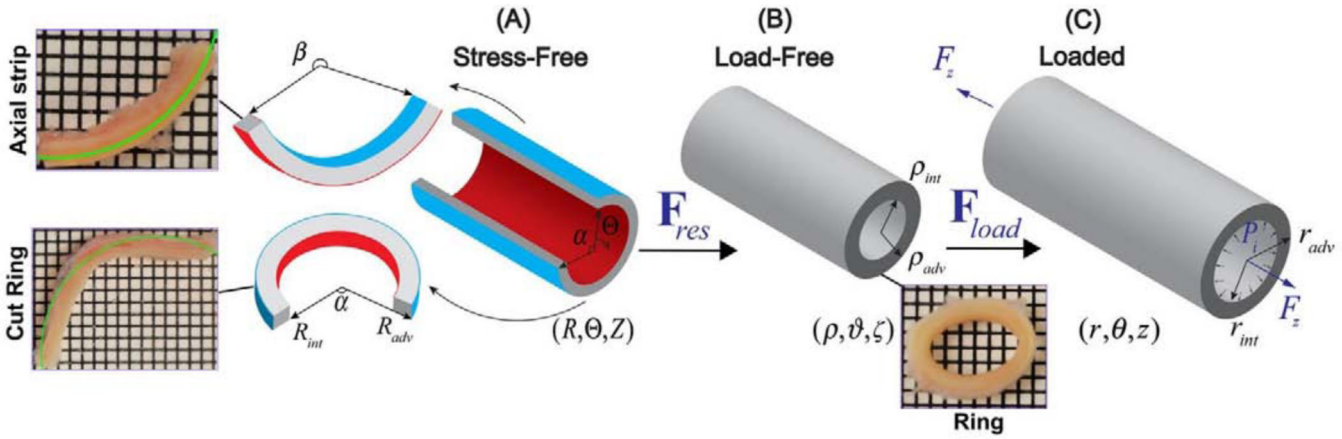

Figure 2:

Kinematics of the artery demonstrating (A) *stress-free* configuration obtained by radially opening the artery into a sector, and cutting out a longitudinal strip, (B) *load-free* configuration with no internal pressure or longitudinal pre-stretch, and (C) the *in vivo loaded* state. Note that in the *stress-free* state, the longitudinal strip curves intimal outward[52], while the radially-cut ring curves intimal inward. The grid size in the inserts is 1mm. Green overlaid circles were used for morphometric analysis.

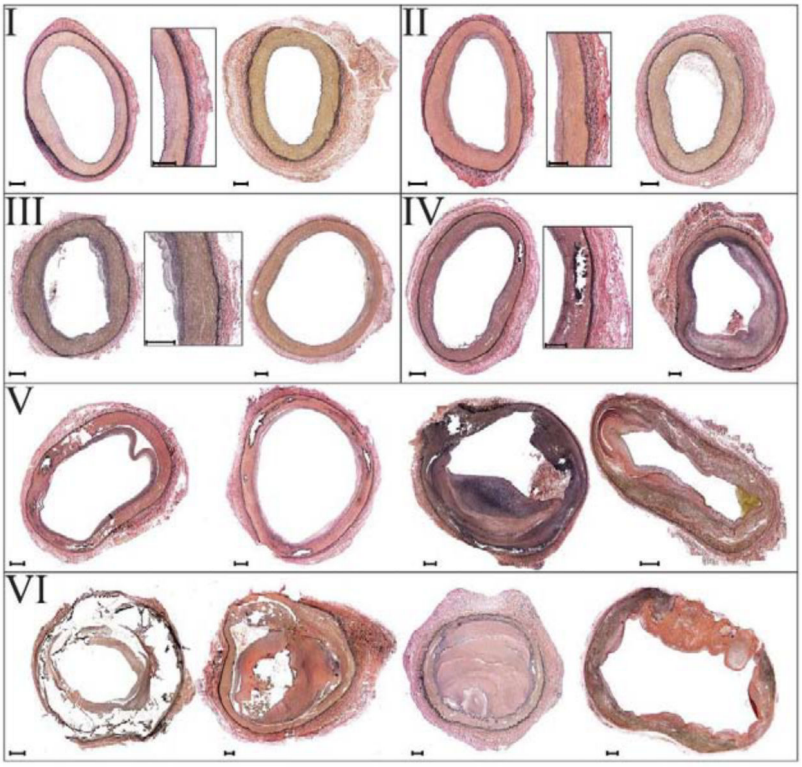

Figure 3:

Six-stage FPA pathology classification scale[43,44] using transverse sections of the artery. Stage I represents healthy arteries with no intimal thickening, no lipid pools, and no calcification; stage II includes arteries with minor intimal thickening and some SMCs proliferation, but no protruding plaques; stage III arteries have plaques with minor protrusion into the lumen, and possibly small pools of extracellular lipid, but no calcium; stage IV represents samples with minor calcification, protruding plaque with <30% stenosis, and moderate pools of extracellular lipid; stage V includes arteries with severe medial calcification, stenosis >75%, or enlarged diameter consistent with early aneurysm formation, and possibly large pools of extracellular lipid; stage VI represents the most severely diseased arteries with extremely calcified arterial medial layer, total vessel occlusions, or fully-developed aneurysms[43,44]. Verhoeff-Van Gieson (VVG) stain: elastin is black, collagen is red, smooth muscle is brown. Several examples are provided for each stage. The scale bars at the bottom left corner of each section represent 500μm.

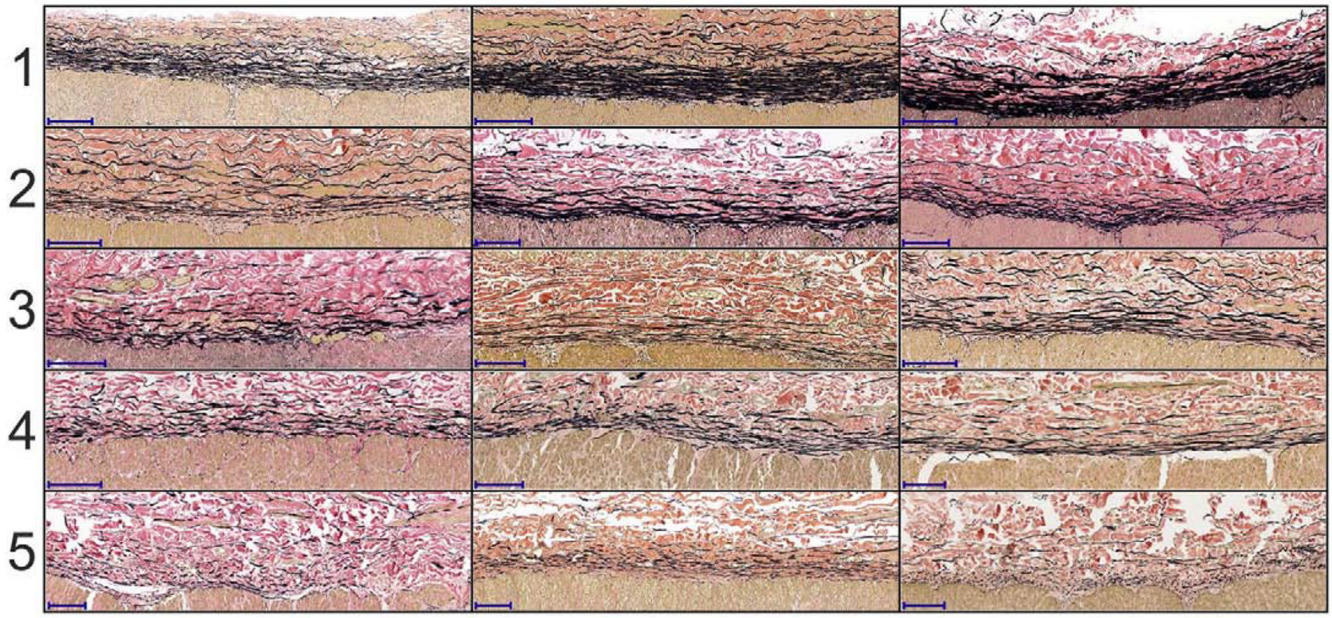

Figure 4:

Five-stage elastic fiber discontinuity scale using longitudinal sections of the artery. The scale ranges from 1 (continuous fibers) to 5 (discontinuous fibers). Several examples are provided for each stage to illustrate variability. Elastic fibers are in the external elastic lamina (EEL) at the border of media and adventitia. Verhoeff-Van Gieson (VVG) stain: elastin is black, collagen is red, smooth muscle is brown. The scale bars at the bottom left corner of each section represent 100μm.

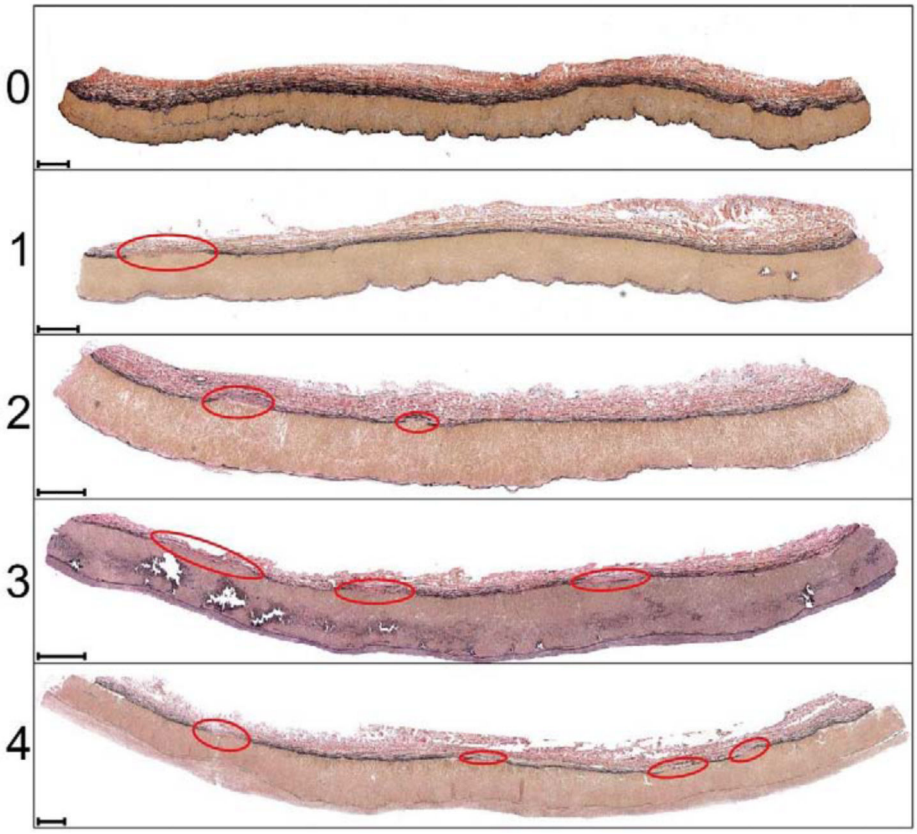

Figure 5:

Major breaks in the external elastic lamina (EEL) assessed using longitudinal sections. The breaks are highlighted with red ellipses, and the number of breaks is shown on the left. Verhoeff-Van Gieson (VVG) stain: elastin is black, collagen is red, smooth muscle is brown. The scale bars at the bottom left corner of each section represent 500μm.

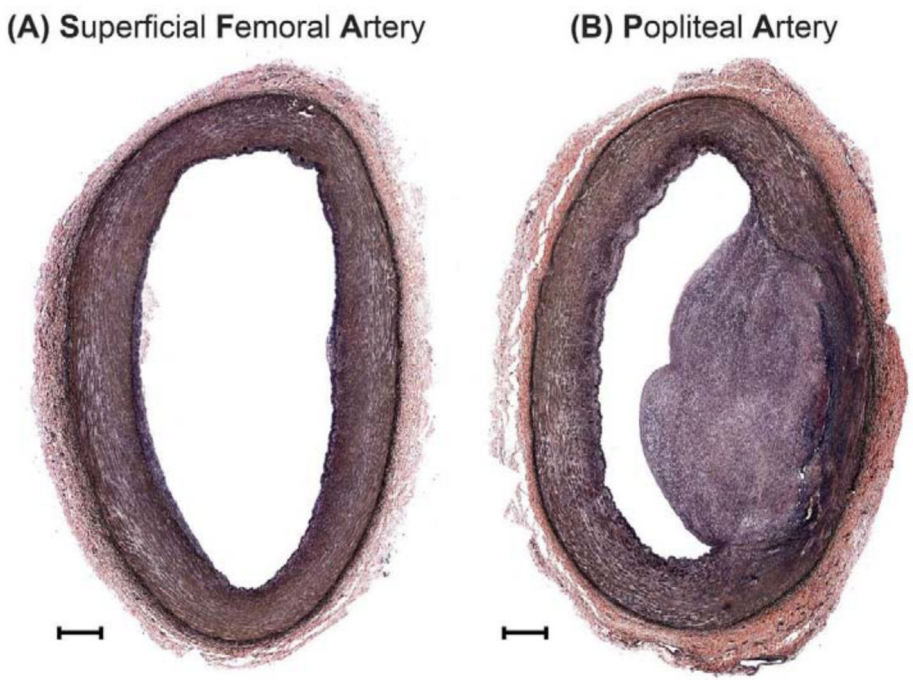

Figure 6:

VVG-stained cross-sectional image of the (A) proximal superficial femoral artery (SFA), and (B) distal popliteal artery (PA) from the same 38-year-old male donor. Note the fibrous plaque in the PA but no gross pathology in the SFA. The scale bars at the bottom left corner of each section represent 500μm.

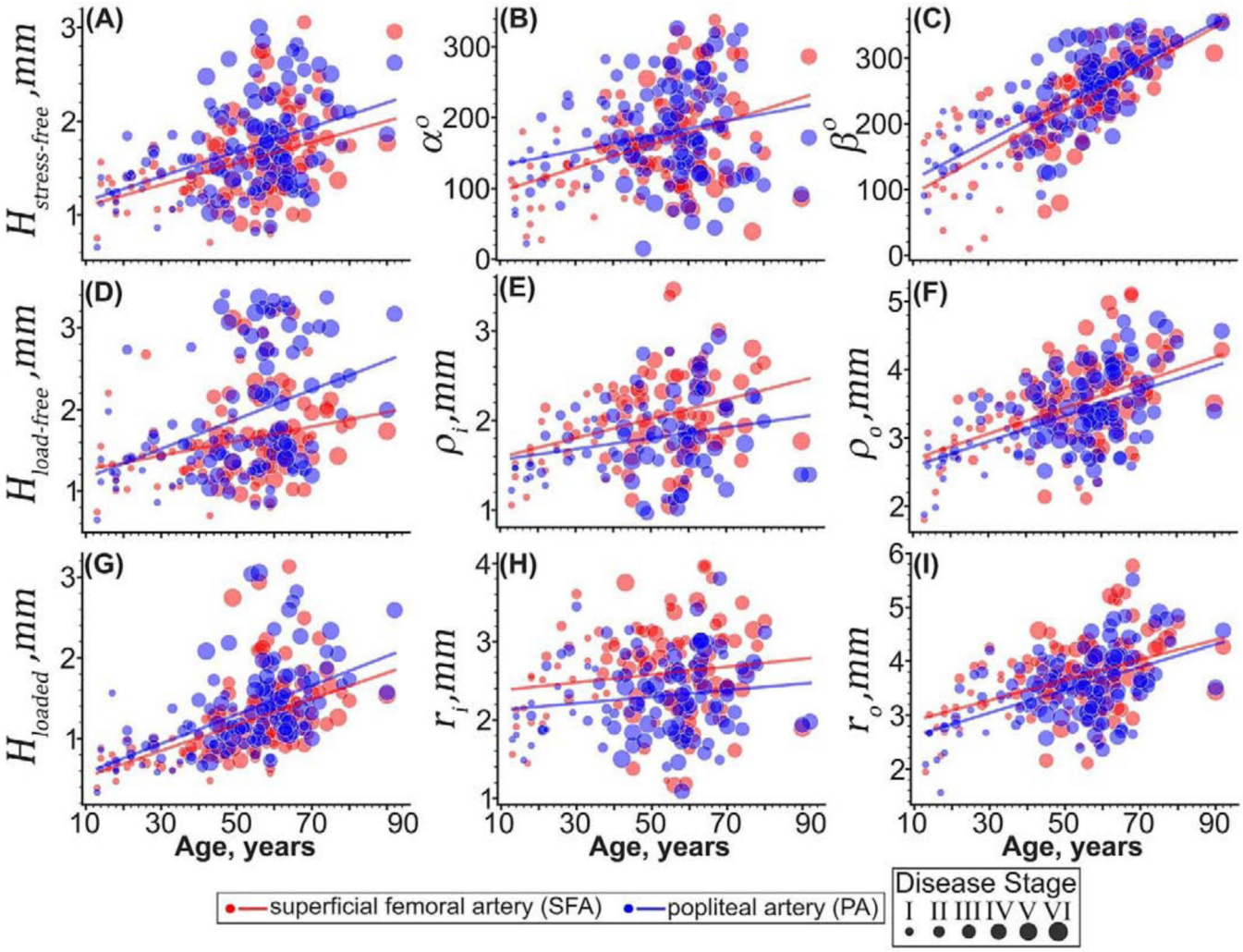

Figure 7:

Morphometric characteristics of the superficial femoral (SFA, red) and popliteal (PA, blue) arteries plotted versus age. Panels include arterial wall thickness in the (A) *stress-free* (H) *load-free*, and (G) *loaded* configurations; (B) circumferential (α) and (C) longitudinal (β) opening angles; *load-free* (E) inner and (F) outer radii; and *loaded* (H) inner and (I) outer radii. The size of the dots represents the disease stage of each specimen, with larger dots indicating more disease. Lines are linear regression fits to the experimental data.

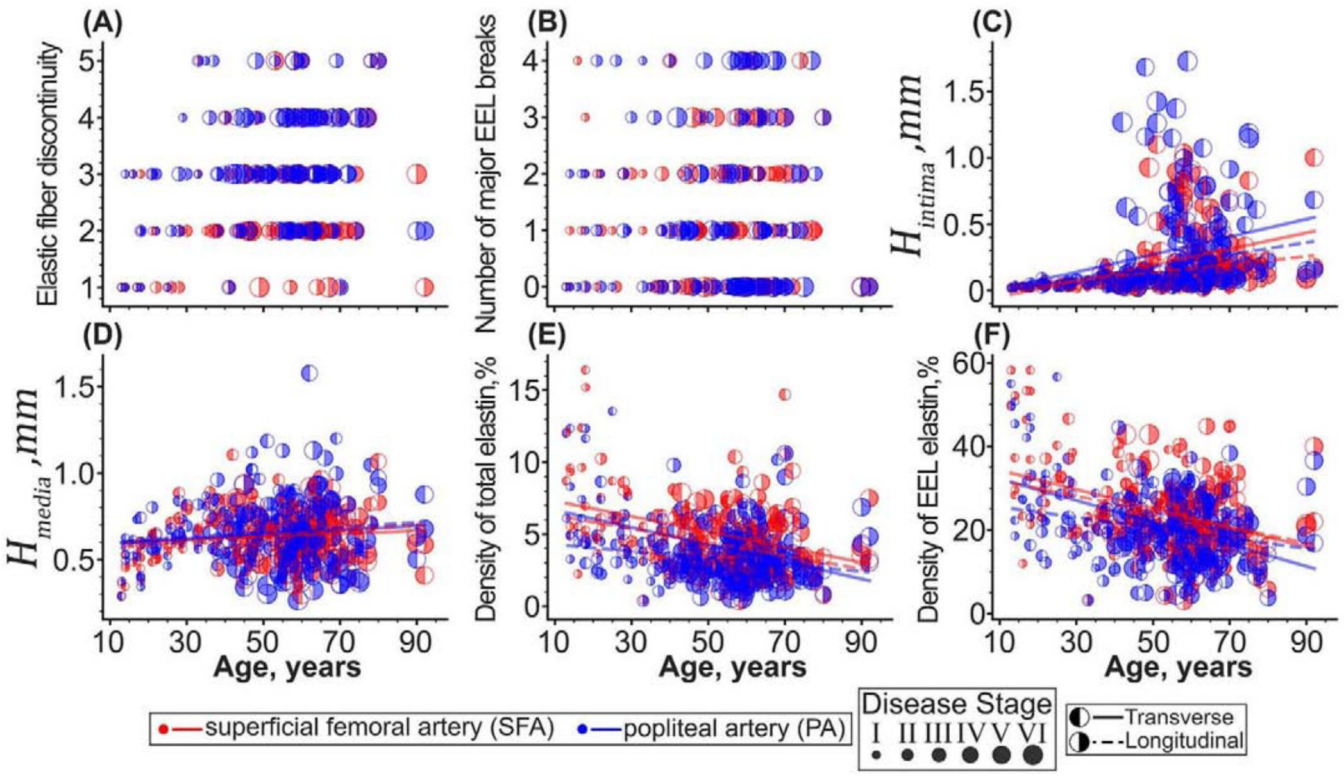

Figure 8:

Changes with age in (A) the discontinuity of elastic fibers in the EEL, (B) the number of major EEL breaks, (C) thickness of the tunica intima, (D) thickness of the tunica media, (E) density of the total elastin, and (F) density of elastin in the EEL of the SFA (red) and PA (blue) measured using transverse (left-filled dots) and longitudinal (right-filled dots) sections. The size of the dots represents the disease stage with larger circles corresponding to a more advanced disease stage. Lines are linear regression fits to the experimental data.

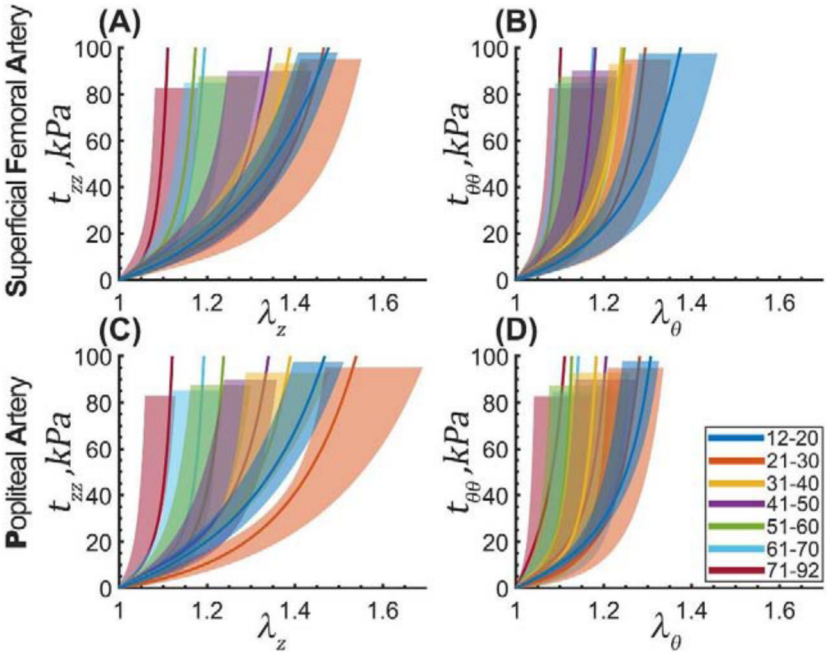

Figure 9:

Median equibiaxial stress-stretch curves for the SFA (top) and PA (bottom) separated into 7 decadal age groups. Panels (A) and (C) plot longitudinal stretch versus longitudinal Cauchy stress, and panels (B) and (D) report circumferential stretch versus circumferential Cauchy stress. Legend summarizes the range of ages for each group (years). Variability within each age group is demonstrated by the shaded semi-transparent regions that bound 25th and 75th percentile ranges. They have different heights for better visualization.

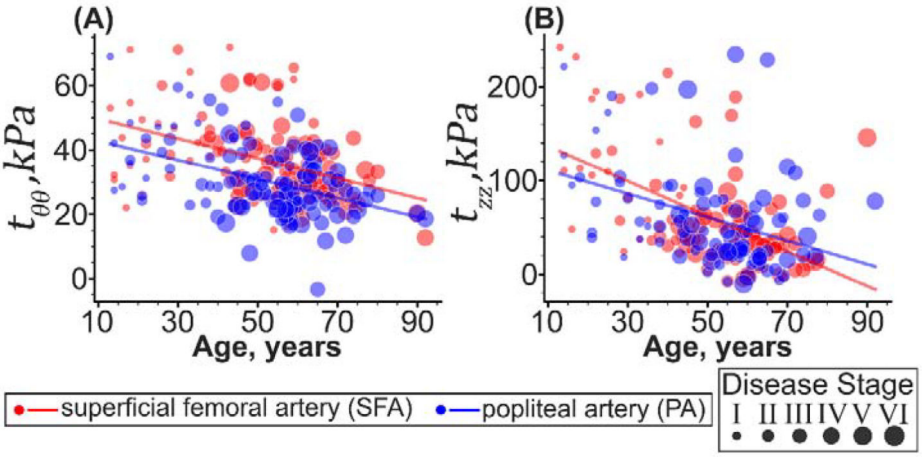

Figure 10:

Changes in (A) circumferential and (B) longitudinal physiologic stresses with age in the SFA (red) and PA (blue). The size of the dots represents the severity of the vascular disease, with larger dots indicating more advanced disease stage. Lines are linear regression fits to the experimental data.

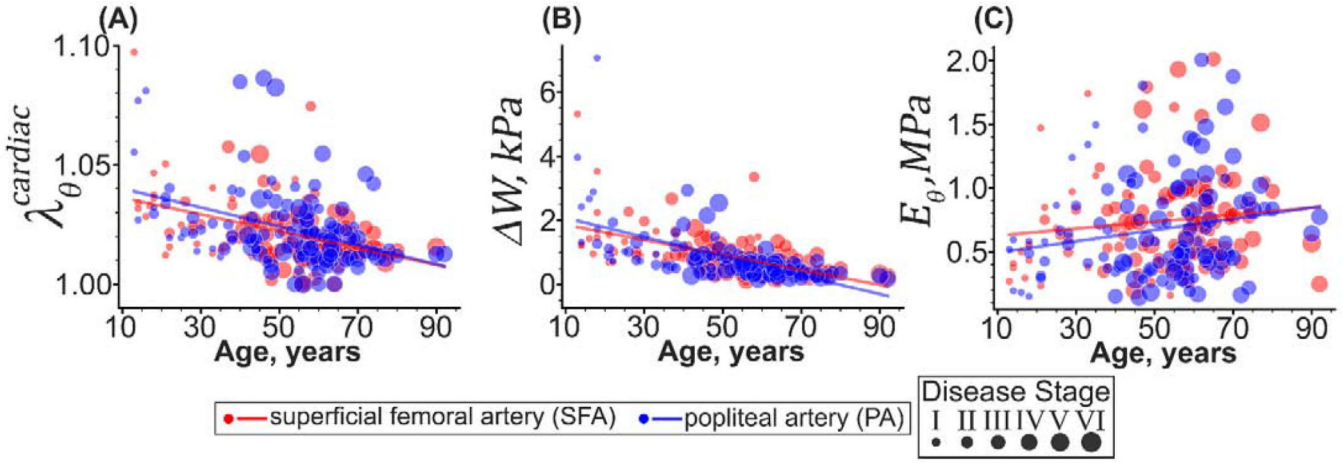

Figure 11:

Changes with age in (A) circumferential stretch, (B) stored elastic energy, and (C) circumferential stiffness over the cardiac cycle as the SFA (red) and PA (blue) deform from diastole (80mmHg) to systole (120mmHg). The size of the dots represents the severity of the vascular disease, with larger dots indicating more advanced disease stage. Lines are linear regression fits to the experimental data.

Table 1:

Subject demographics, risk factors, and vascular pathology stage for specimens in 7 decadal age groups. Pathology was quantified on a I to VI scale with I representing healthy and VI severely diseased arteries (Figure 3).

Age group (years)	n	Males, %	Current/ Former smokers, %	BMI (average ± SD)	HTN, %	DM, %	Dyslipidemia, %	CAD, %	SFA Pathology Stage I/II/III/IV/V/VI, %	PA Pathology Stage I/II/III/IV/V/VI, %
16±2 (12–20)	8	62	0/0	20±5	0	0	0	0	100/0/0/0/0/0	87/13/0/0/0/0
26±4 (21–30)	10	70	30/20	28±5	10	10	10	0	50/50/0/0/0/0	30/60/10/0/0/0
37±2 (31–40)	10	80	30/30	33±6	40	20	10	0	40/30/30/0/0/0	20/50/20/10/0/0
46±3 (41–50)	21	71	48/10	34±8	57	19	14	14	10/24/24/14/0/29	0/33/19/14/14/19
57±3 (51–60)	36	61	44/11	32±6	47	33	28	8	8/25/19/11/31/6	0/17/22/22/28/11
64±3 (61–70)	30	80	27/17	33±6	70	27	20	3	0/20/17/40/20/3	0/10/23/23/37/7
76±7 (71–92)	10	80	30/30	31±6	90	50	40	30	0/0/10/40/30/20	0/0/10/40/40/10

n: number of subjects in each age group, BMI: body mass index, HTN: hypertension, DM: diabetes mellitus, CAD: coronary artery disease

Table 2:

Parameters for the four-fiber family constitutive model describing the median response of human SFAs in 7 decadal age groups. A total of 19 different loading protocols were used to determine the constitutive parameters for this model. The coefficient of determination $R^2 \geq 0.99$ for all age groups.

Age group (years)	C_{gr}, kPa	C_1^1, kPa	C_2^1	C_1^2, kPa	C_2^2	$C_3^2 = C_4^2$, kPa	$C_3^2 = C_4^2$	γ°
16±2 (12–20)	2.59	21.52	0.12	8.37	1.59	6.30	1.31	55.53
26±4 (21–30)	5.25	12.63	0.45	3.47	3.84	3.46	2.43	57.54
37±2 (31–40)	4.16	14.50	0.66	9.05	5.09	5.41	3.40	55.88
46±3 (41–50)	5.36	13.78	1.39	17.02	7.40	4.19	7.07	53.88
57±3 (51–60)	4.50	20.33	2.83	13.54	10.01	5.31	10.88	50.67
64±3 (61–70)	4.79	18.60	5.89	11.23	12.68	4.44	18.39	47.33
76±7 (71–92)	0.00	28.38	15.16	15.18	18.43	10.42	30.65	45.78

Table 3:

Parameters for the four-fiber family constitutive model describing the median response of human PAs in 7 decadal age groups. A total of 19 different loading protocols were used to determine the constitutive parameters for this model. The coefficient of determination $R^2 \geq 0.99$ for all age groups.

Age group (years)	C_g, kPa	C_1^1, kPa	C_2^1	C_1^2, kPa	C_2^2	$C_3^2 = C_4^2$, kPa	$C_3^2 = C_4^2$	γ°
16±2 (12–20)	0.02	23.27	0.18	0.57	6.21	19.11	1.24	65.71
26±4 (21–30)	3.32	8.61	0.32	2.00	5.83	4.74	2.92	64.45
37±2 (31–40)	9.51	11.26	1.03	8.48	10.79	3.08	7.48	58.89
46±3 (41–50)	3.25	17.83	1.56	22.45	5.34	5.80	6.94	51.13
57±3 (51–60)	4.66	19.61	3.68	9.51	14.31	4.85	14.98	49.05
64±3 (61–70)	3.49	16.84	7.33	9.02	13.17	4.24	20.49	50.39
76±7 (71–92)	0.00	89.47	23.42	33.66	17.94	16.00	42.52	49.12